DESIGNING THE HUMAN-POWERED HELICOPTER: A NEW PERSPECTIVE

A Thesis

presented to

the Faculty of California Polytechnic State University,

San Luis Obispo

In Partial Fulfillment

of the Requirements for the Degree

Master of Science in Aerospace Engineering

by

Gregory Hamilton Gradwell

June 2011

ii

COMMITTEE MEMBERSHIP

TITLE: Designing the Human-Powered Helicopter: A New
                              Perspective

AUTHOR: Gregory Hamilton Gradwell

DATE SUBMITTED: May 2011

COMMITTEE CHAIR: Dr. Rob McDonald, Associate Professor

COMMITTEE MEMBER: Dr. Kurt Colvin, Professor

COMMITTEE MEMBER: Dr. Jordi Puig-Suari, Professor

COMMITTEE MEMBER: Mr. Pete Muller

ABSTRACT

Designing the Human-Powered Helicopter: A New Perspective

Gregory Hamilton Gradwell

The concept of human-powered vertical flight was studied in great depth. Through the manipulation of preexisting theory and analytical methods, a collection of design tools was created to expediently conceptualize and then analyze virtually any rotor. The tools were then arranged as part of a complete helicopter rotor design process. The lessons learned as a result of studying this process—and the tools of which it consists—are presented in the following discussion. It is the belief of the author that by utilizing these tools, as well as the suggestions that accompany them, future engineers may someday build a human-powered helicopter capable of winning the Sikorsky Prize.

TABLE OF CONTENTS

LIST OF TABLES

LIST OF FIGURES

NOMENCLATURE

Name	Definition	Units
c	chord	ft
g	gravitational constant	ft/sec^2
k_b	blade coefficient	
k_G	ground effect coefficient	
m	mass	$slugs$
$\dot{m}$	mass flow rate	$slugs/sec$
r	rotor radial station	
z	height above ground	ft
A	rotor disc area	ft/sec^2
A_b	rotor blade area	ft/sec^2
C_d	drag coefficient	
$\bar{C}_d$	blade mean drag coefficient	
C_l	sectional lift coefficient	
$\bar{C}_l$	blade mean lift coefficient	
C_{l_0}	lift coefficient, $\alpha=0$	
C_L	total lift coefficient	
C_{l_α}	sectional lift curve slope	$1/rad$
C_P	coefficient of power	
C_T	coefficient of thrust	
D	propeller diameter	ft
I	moment of inertia	ft^4
M	bending moment	$ft-lbf$
N	number of rotor blades	
P	power required	W
R	rotor radius	ft
T	thrust	lbf
T_{LOSS}	thrust percentage lost due to coning	
V_T	rotor tip speed	ft/sec
W	helicopter weight	lbf
α	angle of attack	rad
β	coning angle	rad
η_{MECH}	total mechanical efficiency	
η_P	tip propeller efficiency	
θ	rotor twist	rad
λ	inflow ratio	
ν	rotor disc inflow velocity	ft/sec
ρ	air density	$slugs/ft^3$
σ	rotor solidity	
Λ	taper ratio	
Ω	rotor rotation speed	rad/sec

Introduction

The ideas presented in the proceeding pages are new. This is not because they are brilliant or revolutionary, or even necessarily useful in a practical sense; rather their uniqueness springs from the problem that they are trying to solve: human-powered vertical flight. The many obstacles standing in between man and this goal require one to reexamine the most basic of theories that are presented in every helicopter design textbook. This is a war that is fought in the trenches. That is not to say that one mustn't have a firm grasp of the overarching concepts governing rotary wing flight. However, the margins for error here are so small that one must examine every aspect of the design in great detail so that the maximum performance can be extracted from each decision.

If there is one thing that should be taken away from this document, it is that mechanical power should be treated as a currency. It is earned by the pilot and spent by the designer. There are four performance characteristics that can be purchased with this currency: thrust, stability, controllability, and strength. Of these, thrust is the only one with a clear threshold requirement: the rotor must be able to lift its own weight as well as the weight of the pilot. Beyond that, it is up to the designer to set the requirements and then fulfill them.

Over the course of this paper a design process will be presented; one that is believed to offer the best chance of creating a human-powered helicopter capable of capturing the ever-elusive Sikorsky Prize. The keyword here is "create". It is one thing to design the perfect helicopter. But to design one that can actually be built—and built under reasonable time and cost restrictions—is a completely different matter. With each

decision there will be aerodynamic and structural consequences, and often they will be opposing in nature. That which is stronger is rarely lighter, and that which is optimal is rarely simple. While the in-depth topics discussed here will generally deal with aerodynamic principles, the structural implications will never be forgotten. However, the structural design of the helicopter will be left for another time.

But before delving into the depths of the following work, let us first be introduced to the motivation behind this entire operation.

The Sikorsky Prize

Established in 1980 by the American Helicopter Society[1], the Sikorsky Prize was created to motivate the first successful flight of a human-powered helicopter. The rules of the contest state that the aircraft must demonstrate the capability to hover for at least 60 seconds. At some point during that flight the lowest part of the vehicle must reach a height of 3 meters, all while staying within the confines of a 10-meter square. The attempt shall be made on level ground, with a mean wind speed of no greater than 1 meter per second.

The purse was initially set at $20,000. Since its inception there have been two vehicles to successfully demonstrate the ability to hover, however neither was able to achieve the height or duration targets. After a lull of 15 years, the prize was increased to $250,000 in August of 2009 with the hopes of spawning new interest in the endeavor. It was this action that spurred a group of students at California Polytechnic State University, San Luis Obispo to pick up where their predecessors had left off and begin the journey toward human-powered vertical flight.

Previous Efforts

In 1989, after several years of effort and three complete helicopters, Cal Poly, SLO made history with the world's first human-powered helicopter flight[1]. They stayed aloft for 8 seconds and reached a height of 8 inches. The many lessons learned over the life of this program were captured in several senior projects, now housed at Cal Poly's Kennedy Library. Their record-setting aircraft, christened the *Da Vinci III*, consisted of two rotor blades driven by propellers at the rotor tips. The pilot was situated underneath the rotor blades, which placed the blades several feet above the ground. Figure 1 shows a schematic of the aircraft[2].
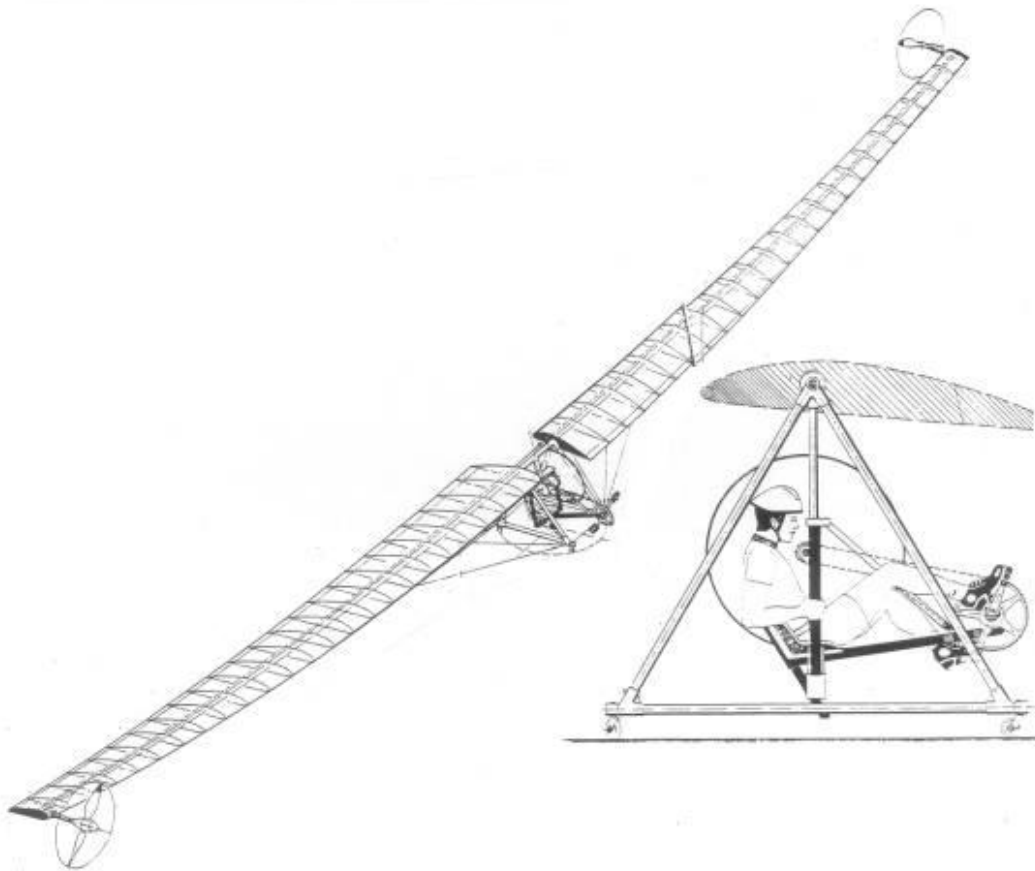
Figure 1: *Da Vinci III*

The single rotor disc configuration of *Da Vinci III* allows for a large disc area, which can lead to a diminished power requirement. However, with only two blades moving at very slow speeds, a small perturbation off of the rotational axis has the potential to significantly disrupt the rotor flight path, as the pitch inertia is very low. As will be shown later, the *Da Vinci III* could have possibly eliminated this instability by placing the pilot above the rotor disc. The other issue of such large blades is that the deflection due to lift will be greater than that experienced by a smaller blade. Not only will this deflection—referred to as "coning"—cause a decrease in lift and an increase in the power requirement, but if it occurs asymmetrically it can contribute to the controllability issues of the aircraft.

Five years after the flight at Cal Poly, a group of students at Nihon University in Japan achieved success with the *Yuri I*, remaining airborne for 19.46 seconds at a height of 8 inches[3]. Their design was much different than *Da Vinci III*, consisting of 4 rotor discs, 5 meters in diameter, driven directly by the pedal crank of the pilot, as seen in Figure 2. Because the discs were situated away from the pilot, they were able to be placed nearly at ground level.

Figure 2: *Yuri I*

Da Vinci III utilized propellers on the rotor tips to drive the rotor, thereby eliminating the problem of a torque that must be counteracted; with four rotor discs, *Yuri I* could drive the rotors directly, as two rotors spun clockwise and the other two spun counterclockwise. The problem of unstable oscillation was also resolved. However the aircraft was still free to translate across the ground, meaning that some sort of control system would most certainly be necessary in order to compete for the Sikorsky Prize. Due to their decreased radius, the rotors would also see less benefit from ground effect, which will be discussed in greater detail in later sections. This aircraft works very well as a sort of hovercraft, but was not proven to be capable of reaching the necessary 3-meter height.

Neither the *Da Vinci* nor *Yuri* machines were equipped with control systems[2,3], meaning they had to rely on their own inherent stability to remain within the confines of the 10-meter-square specified by the Sikorsky Prize rules. As a result, the flights of both vehicles were cut short well before the pilot ran out of power: the Da Vinci due to an unstable pitch/roll oscillation; and the Yuri because it simply ran out of room.

While both of these helicopters exhibited impressive features, it is arguable that neither possessed all the tools necessary to fulfill every objective specified by the Sikorsky Prize. *Da Vinci III*'s main flaw was its instability, and *Yuri I*'s Achilles heel was its diminutive rotor size. Using the lessons learned by these two programs, it is the author's belief that a helicopter can be built that will perform well enough to surpass its predecessors and claim the Sikorsky Prize.

Assuming that one can make the single rotor disc configuration controllable, it seems to hold the advantage in terms of power requirement. But the power costs associated with controlling the single-disc helicopter might end up making it an inferior configuration. Nevertheless, for the sake of consistency, the calculations featured in this paper will pertain to a single-rotor disc helicopter, which will be powered by tip propellers like those used on *Da Vinci III*. However, the theories that appear are applicable to all configurations. Of course, with increasingly complex configurations, there will be physical interactions that are outside the scope of this discussion. But for the design of an individual rotor, which may or may not be part of a multiple-rotor vehicle, the following concepts will be universally relevant.

After introducing the theory behind the process, the analysis methods will be discussed, followed by the design process itself. A short trade study was performed to highlight the effects of several primary rotor parameters. These results are presented and discussed, and should illustrate the effectiveness of the design process in terms of quickly analyzing the performance of several rotor configurations. This paper does not attempt to offer a final helicopter design, but rather it introduces several topics regarding the design of a

human-powered helicopter. If nothing else, the following material should serve as discussion points for future helicopter design efforts.

Let us commence with a brief and selective overview of helicopter theory.

Basic Theory

We will use two different analytical approaches—which should provide a good basis for understanding why a particular rotor behaves the way it does— referred to as momentum theory and blade-element theory. We will begin with momentum theory to introduce the concept of a lifting rotor in general, and then move on to blade-element theory to examine the details pertaining to the individual blades. On occasion, the two methods will be combined in order to produce some useful information.

Momentum theory in hover

Momentum theory[4] applies the basic conservation laws of fluid mechanics to the rotor flow as a whole to estimate the rotor performance. In the momentum theory analysis, the rotor is modeled as an actuator disc, which is a circular surface with zero thickness that causes a pressure difference to accelerate the air through the disc. The actuator disc model is only an approximation to the actual rotor. It is equivalent to considering a rotor with an infinite number of blades. The actual flow through an actuator disc can be very different for a real rotor with a small number of blades, which is why blade-element theory becomes necessary in order to accurately predict the rotor performance.

Let us consider an actuator disc of area A and total thrust T, which appears in Figure 3. Note that we are only examining the case for hover, as with the case of the human-powered helicopter, the rotor will be in a state of hover for essentially the entire flight.
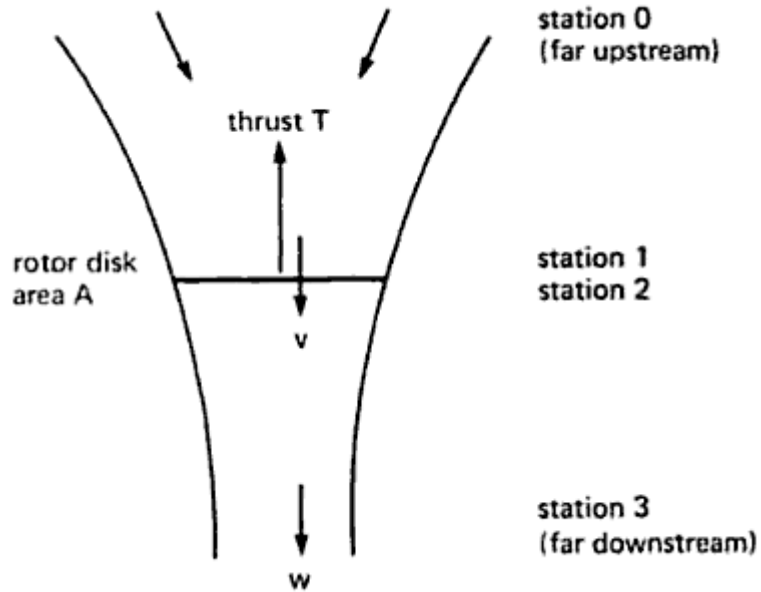
Figure 3: Actuator disc[4]

We can define the mass flux through the disc as follows, where ρ is the air density, A is the area of the actuator disc, and v is the velocity flowing through the disc, referred to as the inflow velocity.

$$\dot{m} = \rho A v \tag{1}$$

It is assumed that the inflow velocity is constant over the entire disc. We will later find that this condition can be achieved with certain twist distribution. By employing the laws of conservation of mass and momentum, we eventually end up with a relationship for the rotor thrust.

$$T = \int 2\rho v^2 dA = 2\rho A v^2 \tag{2}$$

This equation can be rearranged to show the rotor inflow velocity in terms of thrust.

$$v = \sqrt{\frac{T}{2\rho A}} \tag{3}$$

The power required to turn the rotor is separated into two categories, which resemble the two types of drag that a wing experiences in normal flight. Induced power—similar to induced drag—is the power draw that results from the rotor creating thrust. It can be defined by Equation 4.

$$P_i = Tv = T\sqrt{\frac{T}{2\rho A}} \tag{4}$$

Note that for a given thrust, we can decrease the induced power by increasing the rotor disc area. Of course, this is assuming that the rotor has no mass or thickness. In reality, every rotor will have a specific point at which an increase in radius will become detrimental to the performance.

The other kind of power drawn by the rotor is called profile power. It relates directly to the profile drag that is experienced by a wing in that is the power required to move the rotor through the air. However, basic momentum theory assumes that the air is inviscid, meaning that this phenomenon cannot be captured. We will instead have to look to blade-element theory to estimate the profile power requirement. But before we move on, let us first define a few more parameters.

The rotor thrust and power can be expressed in terms of non-dimensional coefficients, which incorporate the rotation speed of the rotor.

$$C_T = \frac{T}{\rho A (\Omega R)^2} \tag{5}$$

$$C_P = \frac{P}{\rho A (\Omega R)^3} \qquad (6)$$

The inflow velocity ratio λ is another useful parameter, which relates the inflow velocity to the rotor tip speed.

$$\lambda = \frac{v}{\Omega R} \qquad (7)$$

Combining Equations 3, 5, and 7, we can relate the inflow velocity to the coefficient of thrust.

$$\lambda = \sqrt{\frac{C_T}{2}} \qquad (8)$$

Recalling the differential form of the thrust in Equation 2, and replacing the thrust with its equivalent coefficient, we can obtain Equation 9.

$$dC_T = 4\lambda^2 r dr \qquad (9)$$

Because we have specified a constant inflow velocity, and hence a constant inflow velocity ratio, we see that the differential thrust coefficient exhibits a triangular distribution. This implies that when a constant inflow velocity through the rotor disc is present, we will see a triangular lift distribution. Conversely, by twisting the rotor to yield a triangular lift distribution, we will force the inflow velocity to be constant over the entire disc.

Using the inflow velocity ratio, we can simplify our induced power equation to one that utilizes the coefficient form.

$$C_{P_i} = \lambda C_T \qquad (10)$$

This relationship becomes important when we evaluate the rotor performance while in ground effect, which will be discussed later. For now we will simply show the

11

relationship between the in-ground effect (IGE) and out-of-ground effect (OGE) values

of the induced power, which is represented by Equation 11. Note that k_G, referred to as

the *ground effect coefficient*, ranges from 0 to 1, with its maximum value corresponding

to the out-of-ground effect condition.

$$C_{P_{i_{IGE}}} = k_G C_{P_{i_{OGE}}} \tag{11}$$

Now let us continue on to blade-element theory, so that we can more precisely define the

aerodynamics affecting the rotating blades.

Blade-element theory in hover

After examining blade-element theory as it pertains to the human-powered helicopter, we

should be able to identify the major factors that contribute to the rotor performance,

allowing us to focus on the aspects of the design that are most critical. To evaluate the

following definite integrals we must make some assumptions about the rotor, so for the

sake of this current discussion it will be assumed that the rotor blades are untapered,

feature a symmetrical airfoil, and are twisted in a way that creates a uniform velocity

inflow through the rotor disc. These equations will be discussed in proceeding sections

with greater detail, but at this point we are looking for a general sense of the factors

governing the performance of the rotor.

As seen before in another form, the rotor thrust can be defined by Equation 12. We now

will define the coefficient of thrust according to Equation 13.

$$T = C_T \rho A (\Omega R)^2 \tag{12}$$

$$C_T = \int_0^1 \frac{\sigma}{2} \left(C_{l_\alpha} \alpha \right) r^2 dr \tag{13}$$

Because the chord is constant, the integral becomes purely a function of r and $C_{l_\alpha}\alpha$, which upon integration results in the following definitions for the rotor thrust coefficient and dimensional thrust, where $\bar{C}_l$ is defined as the blade mean lift coefficient.

$$C_T = \frac{\sigma \bar{C}_l}{6} \tag{14}$$

$$T = \frac{\sigma \bar{C}_l}{6} \rho A (\Omega R)^2 \tag{15}$$

The rotor solidity is defined as the ratio between the rotor blade area and the rotor disc area.

$$\sigma = \frac{A_b}{A} \tag{16}$$

Using this relationship, we can modify the thrust equation to that seen below.

$$T = \frac{A_b \bar{C}_l}{6} \rho (\Omega R)^2 \tag{17}$$

The power required to generate this thrust is defined by Equation 18, using a coefficient of power calculated from Equation 19. The first term corresponds to the induced power C_{P_i}, while the second term is the profile power C_{P_o}.

$$P = C_P \rho A (\Omega R)^3 \tag{18}$$

$$C_P = \int k_G \lambda dC_T + \int_0^1 \frac{\sigma C_d}{2} r^3 dr \tag{19}$$

Using the expression for the velocity inflow ratio that we defined earlier, this power coefficient can be written as Equation 20, and then placed back into the equation for power required. Note that we are assuming a constant mean value for the drag coefficient,

$\bar{C}_d$. This is purely for the sake simplifying the equation. When performing a detailed analysis, the drag coefficient would be calculated at each radial station.

$$C_P = \frac{k_G C_T^{3/2}}{\sqrt{2}} + \frac{\sigma \bar{C}_d}{8} \tag{20}$$

$$P = \left(\frac{k_G C_T^{3/2}}{\sqrt{2}} + \frac{\sigma \bar{C}_d}{8} \right) \rho A (\Omega R)^3 \tag{21}$$

Notice that the first term of the power equation contains the thrust coefficient. We will use Equation 5 to replace the thrust coefficient with its dimensional counterpart.

$$P = \left(\frac{k_G T^{3/2}}{\sqrt{2}(\rho A)^{3/2}(\Omega R)^3} + \frac{\sigma \bar{C}_d}{8} \right) \rho A (\Omega R)^3 \tag{22}$$

Distributing and again utilizing the definition of rotor solidity, we obtain a simplified equation for rotor power required.

$$P = \frac{k_G T^{3/2}}{R\sqrt{2\rho\pi}} + \frac{A_b \bar{C}_d}{8} \rho (\Omega R)^3 \tag{23}$$

The second term of this equation is rather convoluted. By rearranging Equation 17, and substituting, we can obtain Equation 24, which presents the power required in a much more intuitive format.

$$P = \frac{k_G T^{3/2}}{R\sqrt{2\rho\pi}} + \frac{\frac{3}{4}T(\Omega R)}{\frac{\bar{C}_L}{\bar{C}_d}} \tag{24}$$

The human-powered helicopter will essentially spend the entire flight hovering, meaning that the thrust it must create will be equal to the weight of the aircraft. Therefore we can replace the thrust term with a weight term. The second term in this equation corresponds

to the profile power of the rotor. The coefficient of $\frac{3}{4}$ comes from the assumption that the blade consists of a constant chord. This value will change depending on the chord distribution, so it will be replaced with a constant, k_b, referred to hereupon as the *blade coefficient*. The term $\frac{\bar{c}_l}{\bar{c}_d}$ represents the average lift and drag performance of the sectional airfoil. While it is not a precise representation of the actual performance, as the drag coefficient will surely change depending on the lift conditions, it nevertheless helps us visualize the influence the airfoil selection has on the design. From Equation 24 we can identify six different factors that affect the performance of the rotor, which will now be discussed in detail.

Ground effect coefficient, k_G

As the rotor disc approaches the ground, the rotor experiences effects similar to that of an airplane wing in forward flight. The thrust generated by a constant power input increases as the rotor approaches the ground, or conversely, the power required to generate a constant thrust decreases with the diminishing rotor height. This is due to the decrease in induced velocity, which is the source of the induced power required to turn the rotor. The downstream flow also creates a sort of cushion of air beneath the rotor, which in a sense, likens the rotor in ground effect to a hovercraft. Experimentally it is very difficult to measure the induced velocity, and therefore researchers have simply measured the decrease in power required for equivalent thrust as the rotor disc approaches the ground. Several analytical, numerical, and experimental solutions to this ground effect have been offered[5,6,7], with a wide range of results, as portrayed in Figure 4**.**
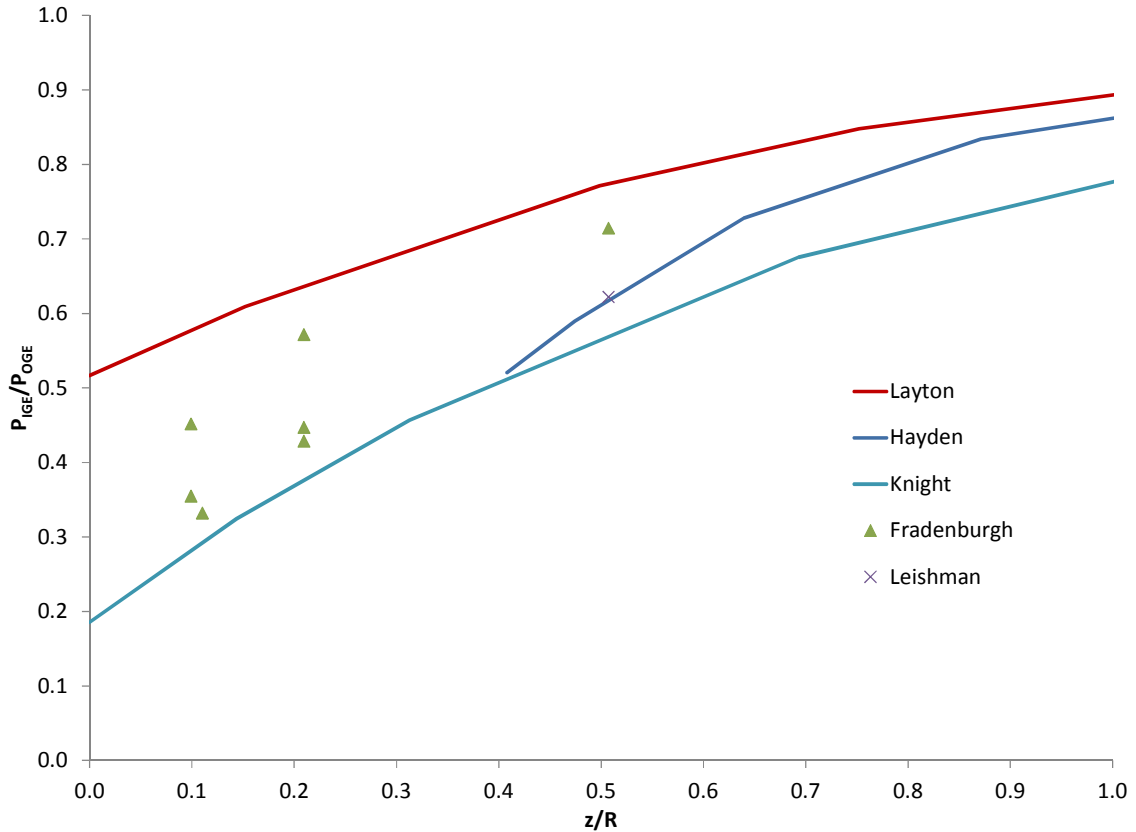
Figure 4: Power reduction due to ground effect

The abscissa represents the ratio of the rotor disc height to the rotor radius. The *Da Vinci III* possessed a z/R value of approximately 0.1 when on the ground and 0.3 when at a height of 3 meters (we can contrast this with *Yuri I*, whose z/R ratio was less than 0.05 when on the ground, but over 0.6 at 3 meters). Flying so low to the ground presents two analytical challenges: there are very few available estimates of the grounds effects, and of these few, there is considerable disagreement in terms of the power reduction caused by the ground. This makes it difficult to confidently estimate the impact of ground effect on the rotor. Furthermore, the value of the ordinate in Figure 4, P_{IGE}/P_{OGE}, is not ideal in terms of the rotor design, as it incorporates the total power reduction, while ground effect is only applicable to the induced power.

The fact that the ground effect is related to the ratio z/R places considerable emphasis on not only the rotor disc placement, but also the rotor radius. This is the reason why *Yuri I* would have had tremendous difficultly reaching an altitude of 3 meters. Even though the rotor discs began nearly on the ground, by the time the helicopter reached its maximum altitude, it would practically be out of ground effect and could realistically require at least three times as much power to operate. As was previously stated, there is considerable disagreement between scholars as to the exact reduction in power it causes, especially as z/R approaches zero. Because the ground effect coefficient is the first step in the design process, the designer must accept the fact that the entire design is based on a parameter that may or may not be accurate.

In 1941 Montgomery Knight and Ralph Hefner published a paper titled "Analysis of Ground Effect on the Lifting Airscrew"[5]. This paper offered an analytical look at ground effect, notably how the induced velocity, thrust, and power were altered as the rotor approached the ground. One of their findings suggested that a velocity inflow that was constant across the span while out of ground effect, would change according to the proximity to the ground. Figure 5 shows the results of this analysis.
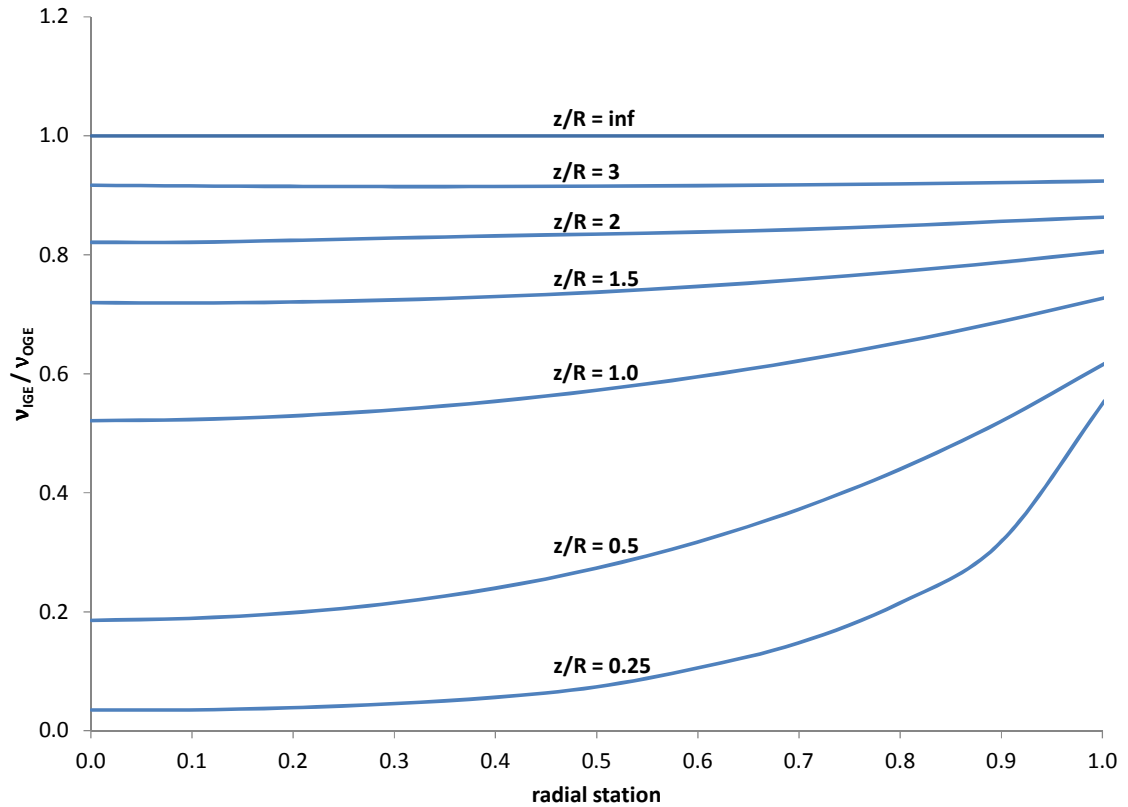
Figure 5: Inflow velocity distribution

We see that the in theory, for small values of z/R, the inflow at the rotor tip is significantly different than that at the root. Since the rotor twist is designed under the assumption that the inflow in constant over the entire span, it will undoubtedly produce a non-optimal solution once the rotor is placed in ground effect. Fortunately the inflow ratio $(v/\Omega R)$ is relatively small, so the discrepancy between the assumed inflow velocity and the actual value might not result in a large error in terms of predicted twist required and subsequently predicted performance. However, as has been stated before, the challenges of the Sikorsky Prize force the helicopter designer to extract every possible ounce of performance from the design, hence this finding may be significant. Again, this was only shown analytically. The rotor might behave differently in flight. In order to

reduce this uncertainty as much as possible, students at Cal Poly have undertaken the task

of creating their own ground effect data through the use of scale rotors. Once their

experiments are complete, they should have a better grasp on the ground effect

coefficient as it relates to the human-powered helicopter.

We now move on to the second dominant factor, total system weight.

Total system weight, W
Recalling Equation 24 (reproduced here), we see that the system weight appears in both

terms of the power required.

$$P = \frac{k_G W^{3/2}}{R\sqrt{2\rho\pi}} + W \frac{k_b(\Omega R)}{\frac{\bar{c}_l}{\bar{c}_d}}$$

The fact that each weight term is taken to a power greater than or equal to unity means

that every percentage of weight gain will result in at least one percent gain of the power

requirement. Keeping the weight to a minimum is no revolutionary concept. However

trying to balance the costs and benefits of changes that result in an increase in weight will

prove crucial. For example, strengthening the spar will make it heavier, but it will also

reduce the rotor coning, which will in turn improve the rotor's thrust and power

performance. The question is, of course, will the better thrust and power results offset the

weight increase? This can only be answered after the rotor design has progressed far

enough to know the several parameters that are involved in the relevant calculations.

Hence as far as preliminary design is concerned, the helicopter must be made as light as

possible. It is desirable for every component to be equally strong as every other

component, so that if there is any sort of failure, the entire structure will fail at once. This

can be accomplished—or at least attempted—by appropriate spar design and construction

as well as suitable rib spacing.

We continue with another primary factor, the rotor radius.

Rotor radius, *R*

From Equation 24 we see that the radius appears in both terms; however, it lies in the numerator in one term and the denominator of the other. Looking purely at the induced power losses, we would like to have the radius be as large as possible, as the induced power exhibits an inverse relationship with the radius. While this means that each additional unit of radius added will decrease the power requirement, it also means that the rate the power diminishes gets smaller as well. If we assume that the rotor rotation speed remains constant while the radius is stretched, we are essentially given three options in terms of how we allow the rotor planform to change. Holding the solidity constant will mean that the rotor scale will be retained. The local chord must increase or decrease proportionally with the radius. We can also hold the blade area constant, which means that the local chord at each radial station will decrease as the radius increases. The third option is to keep the chord constant while the radius is stretched.

Table 1: Increasing rotor radius

Parameter held constant	Local chord response to increase in radius	Local chord response to decrease in radius
Solidity	Increase	Decrease
Blade area	Decrease	Increase
Chord	No change	No change

Table 1 summarizes the planform effects of altering the rotor radius. The radius will also impact the structural performance of the rotor. A larger rotor means that the bending

20

moment experienced along the entire span will increase. Therefore the resulting thrust will either decrease due to a more dramatic deflection, or the spar must be strengthened in order to maintain the current thrust output. Either scenario will result in a power requirement increase to achieve the necessary thrust.

Because of the many complexities involving the rotor radius, it is desirable to keep it fixed for the duration of each complete aerodynamic design process. In other words, one would specify the radius, and then examine the effects of the other variables until arriving at an optimal solution. This process would then be repeated for a range of radii, which would eventually allow the designer to observe the realistic radius effects, having accounted for the structural contributions to the rotor's performance.

Since we have identified the variables that appear in the induced power term, we move to those parameters that affect the profile power, starting with the blade coefficient.

Blade coefficient, k_b

While the induced power of the rotor can be minimized for any geometry though the use of twist, the profile power is dependent on the planform shape of the rotor. A constant-chord blade is the easiest to manufacture, but yields slightly inferior performance in terms of the blade coefficient. As will be shown later, the aerodynamically optimal planform features a chord that decreases nonlinearly from the root to the tip. It is called "optimal" because it allows for the rotor to be twisted in a way such that nearly the entire blade sees the same angle of attack, and therefore the same lift and drag coefficient. Thus, the airfoil could potentially be operating at its optimal point for a majority of the span. While a truly nonlinear taper is nearly impossible to construct, it is reasonable to assume that a

"piecewise-nonlinear" planform could be created by combining several linearly tapered sections.

We can determine the bounds of the blade coefficient by examining the equations for the thrust and profile power coefficients, reproduced from Equations 13 and 19 below.

$$C_T = \int_0^1 \frac{\sigma}{2}(C_{l_\alpha}\alpha)r^2 dr$$

$$C_{P_o} = \int_0^1 \frac{\sigma C_d}{2} r^3 dr$$

Of the rotor planforms that we will analyze, the constant chord rotor will yield the largest blade coefficient. This case was shown in the blade-element theory discussion, but it will be repeated here. For a constant chord, σ is constant, and therefore the thrust and power coefficients reduce to:

$$C_T = \frac{\sigma \bar{C}_l}{6}$$

$$C_{P_o} = \frac{\sigma \bar{C}_d}{8}$$

We showed that the blade coefficient was related to the profile power according to the following relationship.

$$P_o = \frac{k_b T(\Omega R)}{\frac{\bar{C}_l}{\bar{C}_d}} \tag{25}$$

Substituting for the thrust and power, using the above coefficients, we obtain the following equation.

22

$$\frac{\sigma C_{d_0}}{8} \rho A(\Omega R)^3 = \frac{k_b \frac{\sigma C_l}{6} \rho A(\Omega R)^3}{\frac{\bar{C}_l}{\bar{C}_d}} \tag{26}$$

After several cancellations, we again find that the blade coefficient k_b is equal to $\frac{3}{4}$. Now

let us perform the same operations with the optimally-tapered blade, which is defined by

the chord distribution $\sigma = \frac{\sigma_t}{r}$.

When we evaluate the thrust and profile drag coefficients, we obtain Equations 27 and

28.

$$C_T = \int_0^1 \frac{\frac{\sigma_t}{r}}{2}(C_{l_\alpha}\alpha)r^2 dr = \int_0^1 \frac{\sigma_t}{2}(C_{l_\alpha}\alpha)r dr = \frac{\sigma_t \bar{C}_l}{4} \tag{27}$$

$$C_{P_o} = \int_0^1 \frac{\frac{\sigma_t}{r}C_d}{2}r^3 dr = C_{P_o} = \int_0^1 \frac{\sigma_t C_d}{2}r^2 dr = \frac{\sigma_t \bar{C}_d}{6} \tag{28}$$

We solve again for Equation 25.

$$P_o = \frac{k_b T(\Omega R)}{\frac{\bar{C}_l}{\bar{C}_d}}$$

$$\frac{\sigma_t \bar{C}_d}{6} \rho A(\Omega R)^3 = \frac{k_b \frac{\sigma_t \bar{C}_l}{4} \rho A(\Omega R)^3}{\frac{\bar{C}_l}{\bar{C}_d}} \tag{29}$$

This time we find that k_b becomes $\frac{2}{3}$, which is an 11% decrease from the constant chord

blade for an equivalent thrust condition. The rotor designer will have to determine

whether the manufacturing costs of building a tapered rotor will increase the total power

requirement by less than 11% of the profile power. As our trade study will show later,

sometimes the tapered blade might actually perform worse than the non-tapered blade.

23

Another issue that must be considered with the tapered planforms is the size of the chord towards the rotor tip. If the blade area is held constant while the radius is increased, then the chord will correspondingly decrease. If the chord is allowed to become too small, it will be impossible to manufacture the ribs, or they won't be able to support the structure associated with the tip propellers. The outboard sections of the rotor are particularly susceptible to this because they will likely be utilizing thin airfoils that may also be cambered, which will make them already difficult to build. For all these reasons, the planform design is particularly sensitive to the manufacturing capabilities of the design team.

We will now look at the next parameter. While it affects the profile power, the rotor rotation speed also plays a part in the performance of the tip propellers (assuming the helicopter is equipped with them). Both of these aspects will be discussed in the following section.

Rotor rotation speed, Ω

For a given radius, the rotor rotation speed and tip speed form a proportional relationship.

$$V_T = \Omega R \tag{30}$$

The rotor thrust varies with the square of the tip speed, while the power required varies with its cube. Thus, all other factors remaining constant, an increase in tip speed will result in a decrease of the thrust-per-unit-power ratio. If the tip-driven propellers were not a factor, we would want to turn the rotor as slowly as possibly according to the limits of the airfoil. These airfoil limits would be defined by the maximum lift coefficient combined with the drag performance degradation as the Reynolds number decreased. Because the rotor is driven by propellers turning at the tips, we must also factor in the

efficiency of the propellers when considering the total power requirement. For the conditions in which this rotor will be operating, the propellers will experience increasing efficiency as the rotor speed increases. Of course, the magnitude of this increase will be subject to the design of the propeller. Similar to the case of the rotor, we will prefer a propeller with a large diameter turning very slowly. An advantage of a large diameter (D) is that the influence of the rotor tip speed is less than if the diameter were small. We can demonstrate this by examining the relationship between propeller efficiency (η_P) and rotor tip speed[8]. Note that a propeller can be viewed as a rotor in climb. Thus, while in this case we are using the rotor tip speed, in normal circumstances one would simply be referring to this quantity as the incoming flow velocity.

$$V_T = \eta_P \left(\frac{P_{in}}{\pi \rho D^2 (1 - \eta_P)} \right)^{1/3} \tag{31}$$

While Equation 31 cannot be solved for η_P explicitly, we can numerically find a solution. If we examine the behavior of the propeller efficiency for a constant power input (P_{in}) and a range of rotor tip speeds, we can produce Figure 6. This efficiency is assuming that the propeller is perfectly optimal and experiences no induced or frictional losses. While the actual efficiencies will be reduced by a small percentage, the relative performance is sufficiently representative.
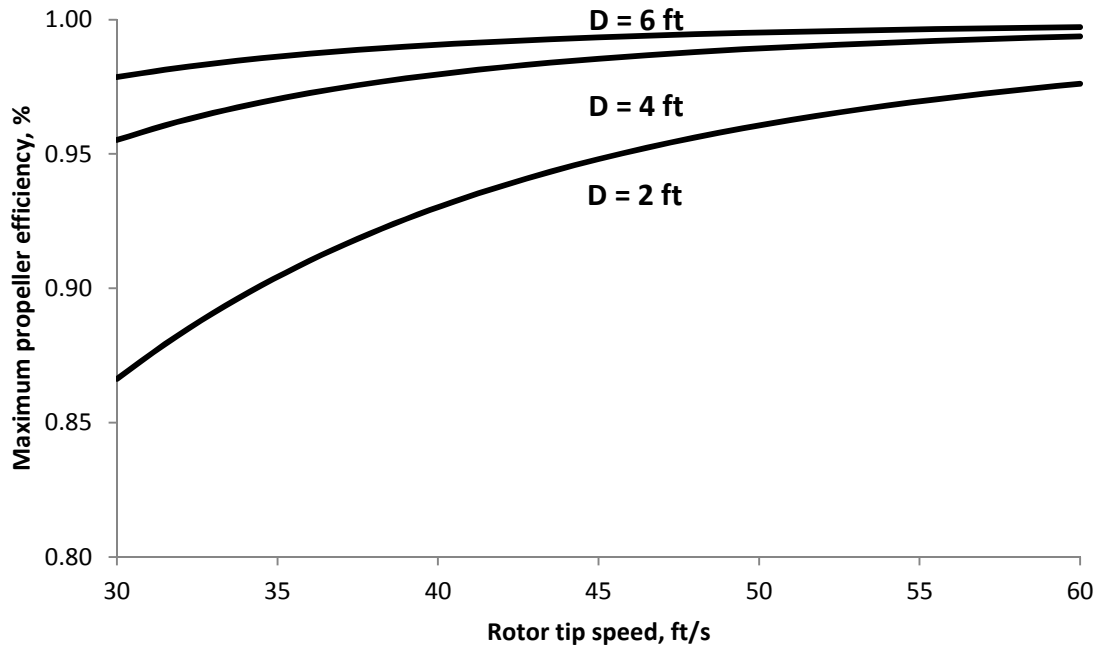
Figure 6: Maximum theoretical propeller efficiency

We see that not only does a larger diameter result in high efficiencies, but the drop-off as the rotor tip speed decreases is much less drastic. A professional cyclist[9] can deliver power outputs upward of 450 W (which would direct 225 W per propeller, assuming no efficiency losses). Let us consider an example: with a diameter of 2 feet, a propeller given a 225-Watt power input could be approximately 98% efficient with an inflow velocity of 60 ft/s, while only achieving 87% efficiency at 30 ft/s. A propeller with a 4-foot diameter will achieve 99% efficiency at 60 ft/s and only be reduced to 95% efficient at 30 ft/s, while the 6-foot diameter propeller goes from nearly 100% to 98% efficient. Thus by simply increasing the tip propeller from 2 feet to 6 feet, we can capture a 9% savings of total efficiency. Considering that only a fraction of this will be lost due to induced and frictional losses, we will see almost of all this savings transfer to the total power requirement.

26

The diameter is limited in magnitude on the upper end by ground clearance issues. However, it is theoretically possible to place the propellers on booms and raise them up as high off the ground as necessary, although this would certainly impact the structural requirements of the rotor. The propeller design essentially is a modified version of the rotor design process, except that it must work within a much smaller design space.

This effect of tip speed is not only relevant at the hover stage; it will impact the propeller performance for the entire wind-up portion of the flight. The greater the propeller efficiency while the pilot is bringing the rotors up to hover rotation speed, the less time the wind-up segment will take, which will leave the pilot more energy for the hover and climb segments. In the same respect, if the hover rotation speed is kept to the minimum possible value, the wind-up time will stay low as well. The seconds that might be eliminated from the total mission time could significantly affect the pilot's ability to achieve a 60-second duration or a 3-meter altitude.

The final parameter from the generalized power equation incorporates lift and drag characteristics of the sectional airfoil. Again, because the lift and drag quantities are only the mean values, we intend only to discuss the consequences of the airfoil selection in general.

Airfoil lift and drag performance ratio, $\frac{\overline{c_l}}{\overline{c_d}}$

The airfoil selection process will affect several aspects of the design besides just the sectional aerodynamic performance. The primary constraint of the airfoil is that it must be manufacturable, and it cannot be so delicate that it will be damaged during assembly or operation. It also must be thick enough to contain the necessary rotor structure. This

eliminates several thin, highly-cambered airfoils that would likely produce the highest

lift-to-drag performance. Because of the tradeoff between aerodynamic and structural

performance, it would be prudent for the designer to hand-select the airfoil for each rib.

For each configuration and rotation setting, the lift coefficient distribution will be known,

as will the local bending moment and Reynolds number. The designer must find an airfoil

that is sufficiently thick, while still yielding suitable drag characteristics for the given lift

coefficient and Reynolds number. For the sake of expedient iteration, it would be suitable

to assign an airfoil to each of several ranges of lift coefficients or Reynolds numbers, but

the final selection process should be completed by hand during the spar design process.

Having looked at these six parameters more closely, we would now like to see an

example of how their variation might influence the rotor performance. A brief analysis

was executed to demonstrate the effects of each parameter on the rotor power. The only

value held constant was the total system weight, which meant that each rotor examined

would be producing the same amount of thrust. First, let us discuss the tool that was

utilized to perform the following analysis, QPROP, as well as the design loop

implemented to minimize the power requirement for each configuration.

QPROP as a design tool

At this point it should be clear that to accurately calculate the rotor performance by hand

for any given configuration would be extremely tedious. Fortunately, a computational

tool that was created to analyze propellers can also be applied to this particular situation.

QPROP, developed by Mark Drela at Massachusetts Institute Technology, uses an

advanced blade-element/vortex theory to predict the thrust and drag characteristics of a

propeller. Of course, by setting the incoming flow velocity to zero, the situation

resembles that of a helicopter rotor in hover. The entire theory that goes into the calculations will not be discussed here, as it is similar to the analytical methods previously identified, but more advanced so as to include three-dimensional effects. Mark Drela's paper entitled "QPROP Formulation"[10] contains the theoretical aerodynamic formulation that is behind the QPROP analysis.

The QPROP code is critical to the design process that will be discussed shortly. A series of MATLAB® scripts were created that are capable of taking a few simple specified rotor parameters and creating an input text file that can be sent to QPROP for analysis. The resulting data is then extracted from an output text file and rearranged for the purpose of fast and simple comparison.

Since we have identified the primary contributors to the rotor performance, we can begin to look at the design process that has been developed for the purpose of finding the optimum rotor solution. A simplified version of the process is shown in Figure 7. This is an iterative process which analyzes the rotor across a range of rotor rotation speeds—hence the loop is referred to as the **OMEGA** loop. The GEOMETRY block takes the inputs and creates a corresponding chord distribution. This, along with the specified ground effect coefficient is fed into the QPROP block, which will determine the twist distribution necessary to achieve the desired thrust. The TIP PROP block factors in the estimated tip propeller efficiency to obtain the total power required. This process is repeated over the given range of rotation speeds and the minimum power case for each configuration is recorded.
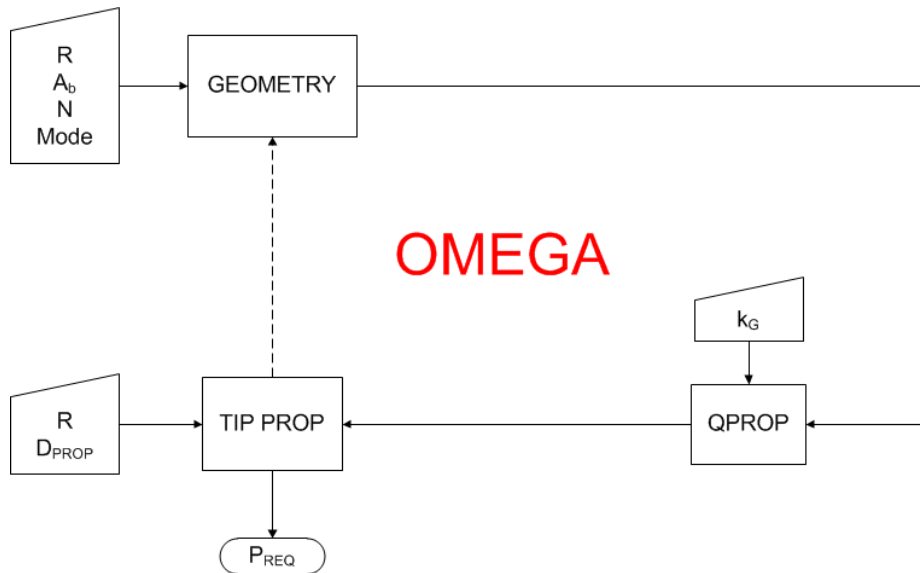
Figure 7: Simplified design loop

Trade Study

As stated before, a trade study was completed to demonstrate how the effects of several factors on the performance of the rotor. From the results of this study, we can gain useful insight in terms of what rotor parameters are the most critical to the design. First, let us look at the configurations that the GEOMETRY block is capable of creating. In essence, there are eight different practical types of taper and twist combinations that collectively form a very broad design space. They are presented in Table 2 below. Note that the terms used to denote these configurations do not necessary describe the actual performance of the rotor, but rather its intended performance, e.g. an ideally twisted blade will not necessarily be the "ideal" solution.

Table 2: Rotor configurations

Mode	Chord Distribution	Twist	Ease of Manufacture
1	Constant	None	Simple
2	Constant	Linear	Simple
3	Constant	Ideal (non-linear)	Moderate
4	Single Taper	None	Moderate
5	Single Taper	Linear	Moderate
6	Optimum taper (non-linear)	None	Moderate
7	Optimum taper (non-linear)	Linear	Difficult
8	Optimum taper (non-linear)	Optimum (non-linear)	Difficult

The following figures show examples of the different types of taper and twist distributions. Figure 8-10 depict top views of a constant-chord blade, single-taper blade, and optimally-tapered blade; all which have the same blade area. It should be noted that the scale of these planforms has been adjusted to emphasis the features of the chord distribution. The aspect ratio of the blades will be much higher in practice. Figure 11 shows the twist distribution for the case with no twist, linear twist, and ideal twist. Note that an optimum twist distribution is not shown. In essence, ideal twist is a specific example of optimum twist, and therefore it was not repeated on the chart. Appendix B discusses how each of these distributions is achieved in much greater detail.
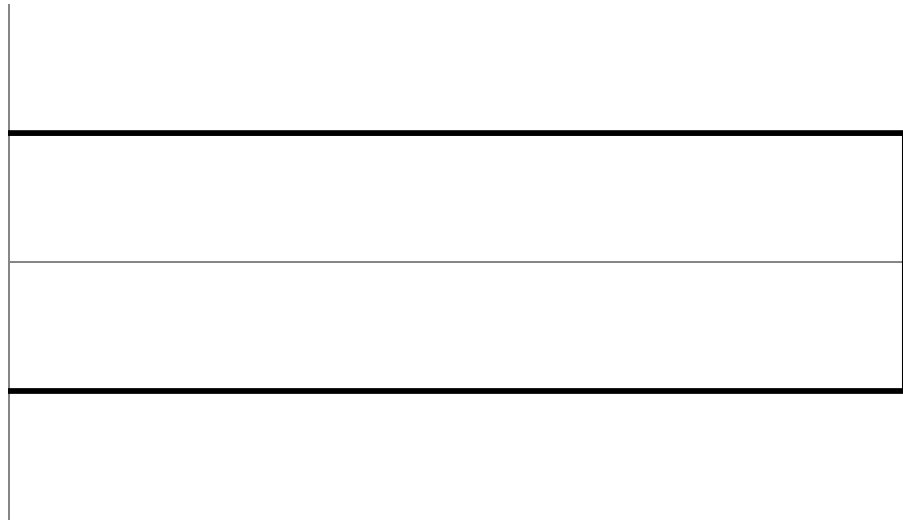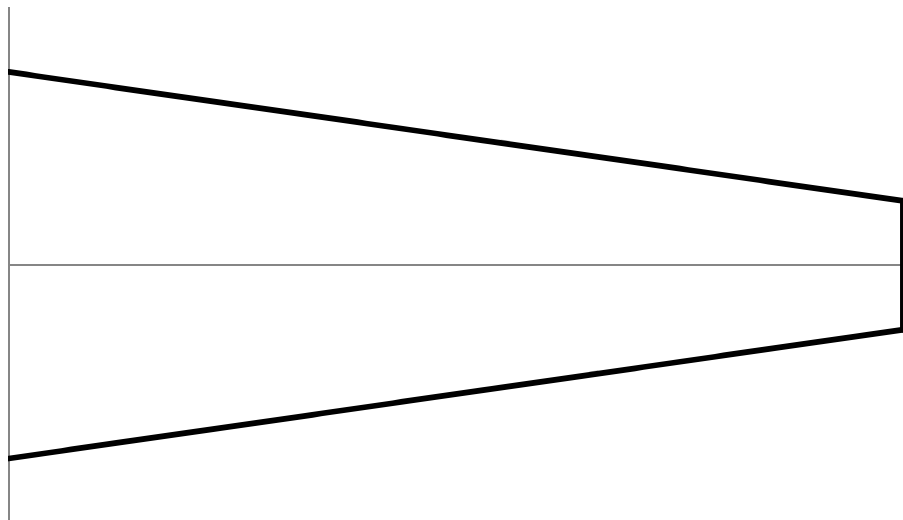
Figure 8: Constant chord planform

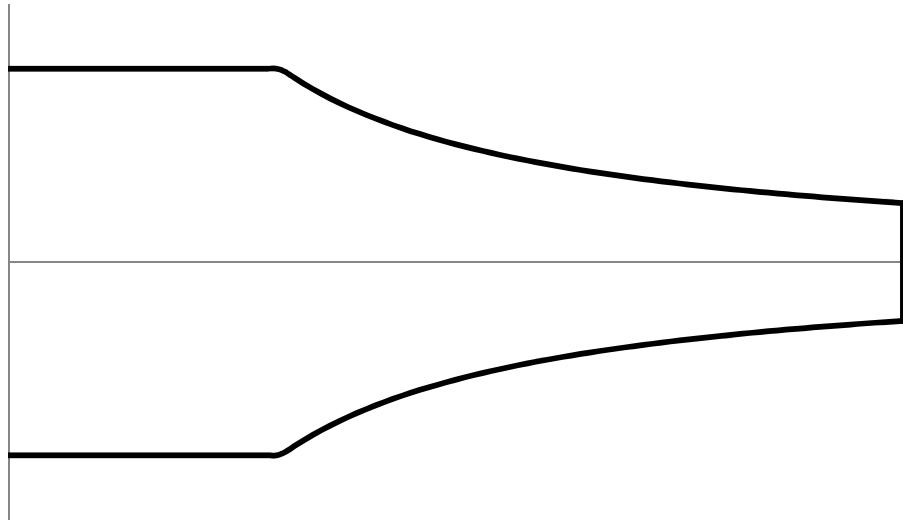

Figure 9: Single-taper planform
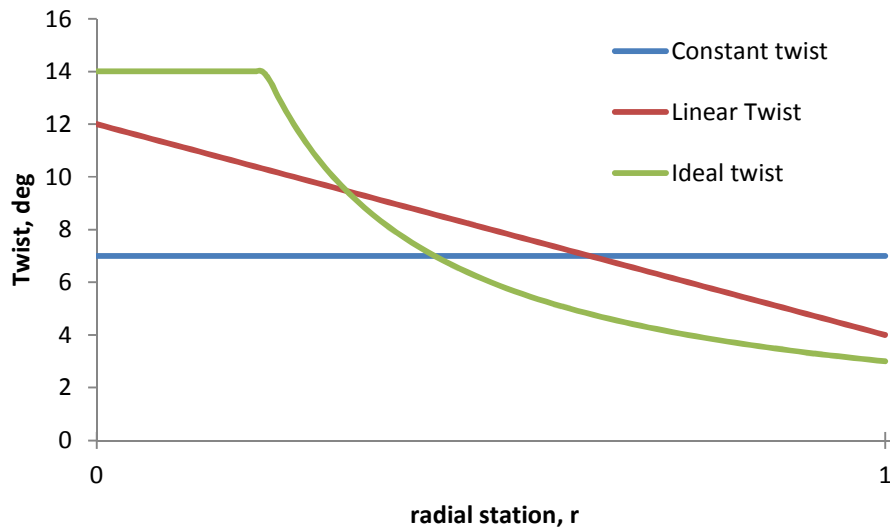
Figure 10: Optimally-tapered planform

Figure 11: Twist distributions

It is important to mention the factor that optimal taper, ideal twist, and optimum twist all feature a segment of constant chord or twist towards the root of the rotor. This is because these cases all approach infinity as r approaches 0. Therefore the rotor designer must select a point at which the chord or twist stops increasing. For the case of taper, the

maximum chord was selected for each rotor so that the section of constant chord began at an r-value of 0.25. The twist for all non-linear cases was limited to 14 degrees.

Table 3 displays the thirty-six different configurations that were analyzed. All

configurations utilize two blades with the same total blade area of roughly 314 ft^2, and

were required to produce 250 pounds of thrust, assuming no thrust was lost to rotor

deflection. Rotor twist was limited to a maximum of 14 degrees. The chord of the

optimally-tapered rotors was not allowed to exceed 3.57 feet for the 50-foot radius rotor

and 5.28 feet for the 75-foot rotor. Profiles of the NACA 0012 and FX 63-137 airfoils

appear in Figure 12 and 13. *Da Vinci III* utilized the FX airfoil for its favorable

aerodynamic performance[12]. The NACA 0012 was selected for analysis simply because it

is a symmetric, reasonably thick airfoil, which should be easier to manufacture than the

cambered FX 63-137, and will produce consistent and predictable lift and drag results.

Table 3: Trade study configurations

| Mode	Radius (ft)	Ground Effect Coefficient	Airfoil
Constant chord, no twist	50	1.0	NACA 0012
Constant chord, no twist	50	0.5	NACA 0012
Constant chord, no twist	50	0.3	NACA 0012
Constant chord, no twist	50	1.0	FX 63-137
Constant chord, no twist	50	0.5	FX 63-137
Constant chord, no twist	50	0.3	FX 63-137
Constant chord, no twist	75	1.0	NACA 0012
Constant chord, no twist	75	0.5	NACA 0012
Constant chord, no twist	75	0.3	NACA 0012
Constant chord, no twist	75	1.0	FX 63-137
Constant chord, no twist	75	0.5	FX 63-137
Constant chord, no twist	75	0.3	FX 63-137
Constant chord, ideal twist	50	1.0	NACA 0012
Constant chord, ideal twist	50	0.5	NACA 0012
Constant chord, ideal twist	50	0.3	NACA 0012
Constant chord, ideal twist	50	1.0	FX 63-137
Constant chord, ideal twist	50	0.5	FX 63-137
Constant chord, ideal twist	50	0.3	FX 63-137
Constant chord, ideal twist	75	1.0	NACA 0012
Constant chord, ideal twist	75	0.5	NACA 0012
Constant chord, ideal twist	75	0.3	NACA 0012
Constant chord, ideal twist	75	1.0	FX 63-137
Constant chord, ideal twist	75	0.5	FX 63-137
Constant chord, ideal twist	75	0.3	FX 63-137
Optimum taper, optimum twist	50	1.0	NACA 0012
Optimum taper, optimum twist	50	0.5	NACA 0012
Optimum taper, optimum twist	50	0.3	NACA 0012
Optimum taper, optimum twist	50	1.0	FX 63-137
Optimum taper, optimum twist	50	0.5	FX 63-137
Optimum taper, optimum twist	50	0.3	FX 63-137
Optimum taper, optimum twist	75	1.0	NACA 0012
Optimum taper, optimum twist	75	0.5	NACA 0012
Optimum taper, optimum twist	75	0.3	NACA 0012
Optimum taper, optimum twist	75	1.0	FX 63-137
Optimum taper, optimum twist	75	0.5	FX 63-137
Optimum taper, optimum twist	75	0.3	FX 63-137
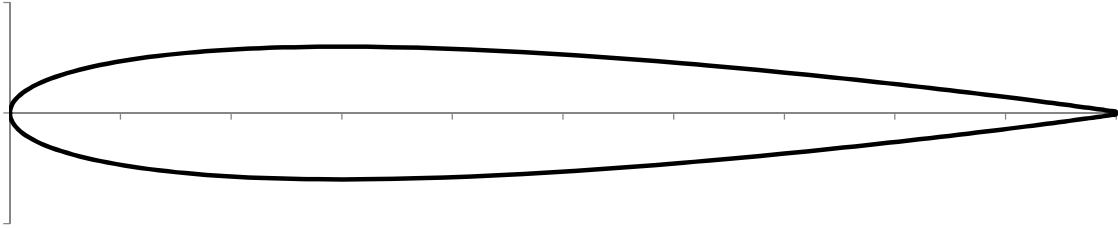
Figure 12: NACA 0012 airfoil[13]
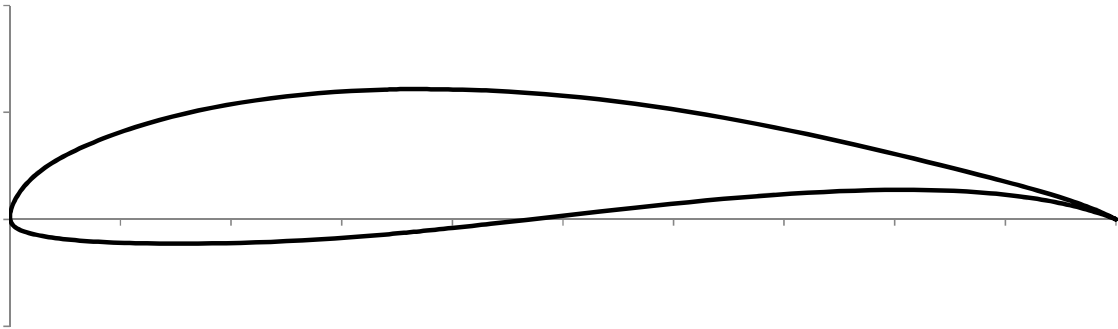
Figure 13: FX 63-137 airfoil[14]

The constant chord, untwisted rotor would likely be the most simple to design and manufacture. By adding ideal twist to the constant-chord rotor, we can theoretically improve the induced power characteristics while keeping the rotor relatively easy to manufacture. If a nonlinear optimum taper is introduced, the rotor becomes more difficult to make, but should theoretically require the least amount of power. However, the results of this study showed that this may not always be the case.

Let us first examine the performance differences between the three rotor modes at each radius/airfoil combination. Figure 14-17 show the power required for each configuration, with three different values assumed for the ground effect coefficient. For each configuration, the rotor speed and twist distribution was varied to find the point at which the rotor could create the necessary thrust with the minimum power required.
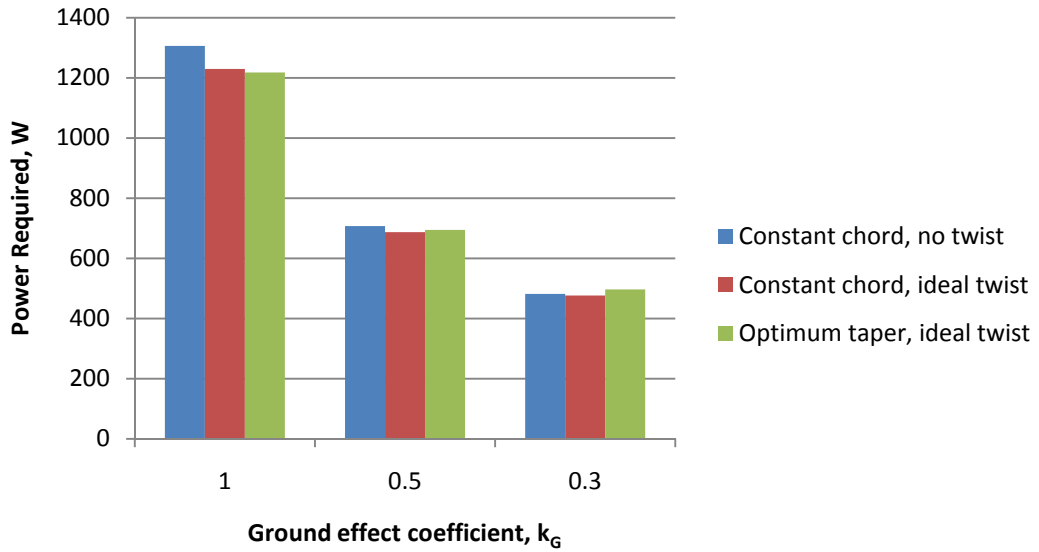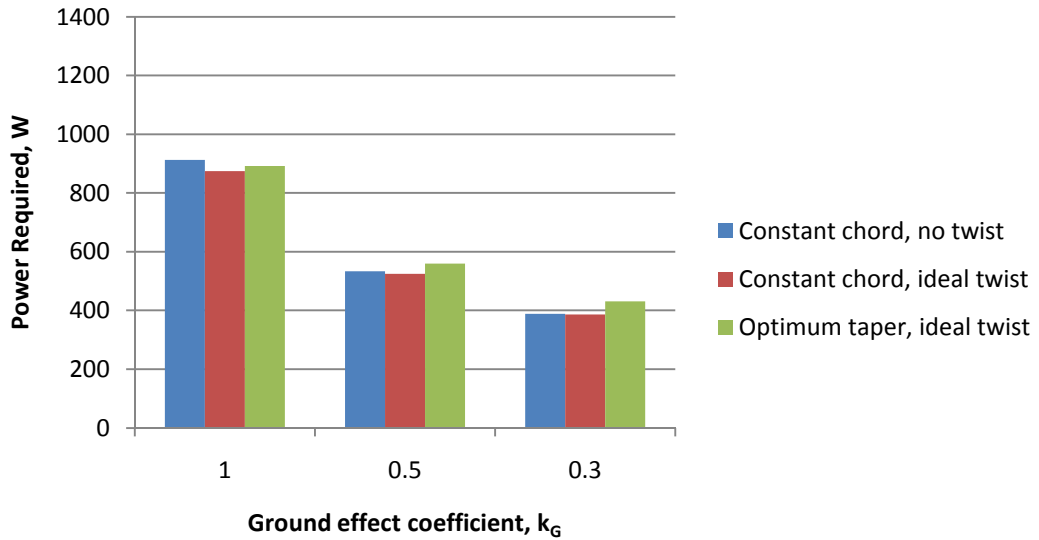
37

Figure 14: Total power required, R = 50 ft, NACA 0012

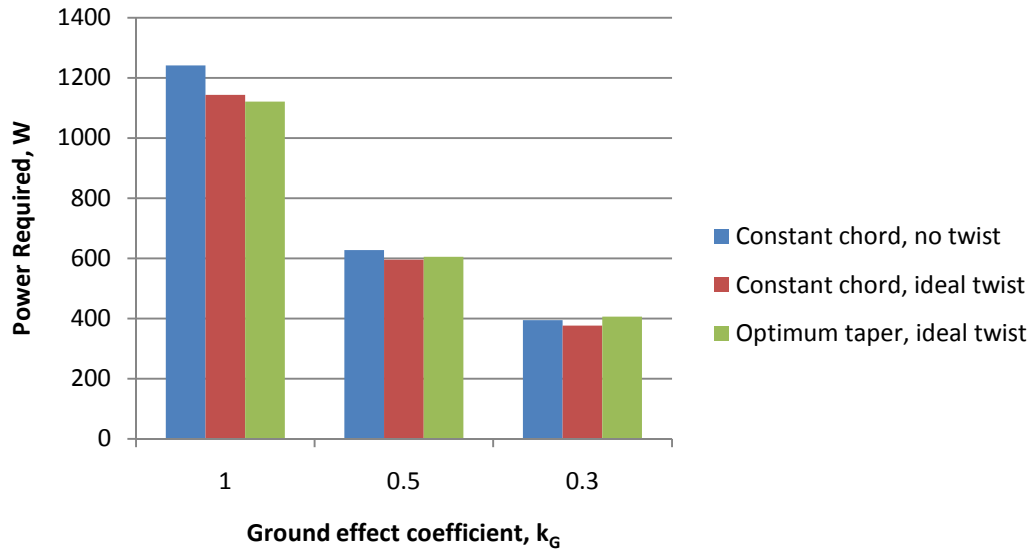**Figure 15: Total power required, R = 75 ft, NACA 0012**

Figure 16: Total power required, R = 50 ft, FX 63-137
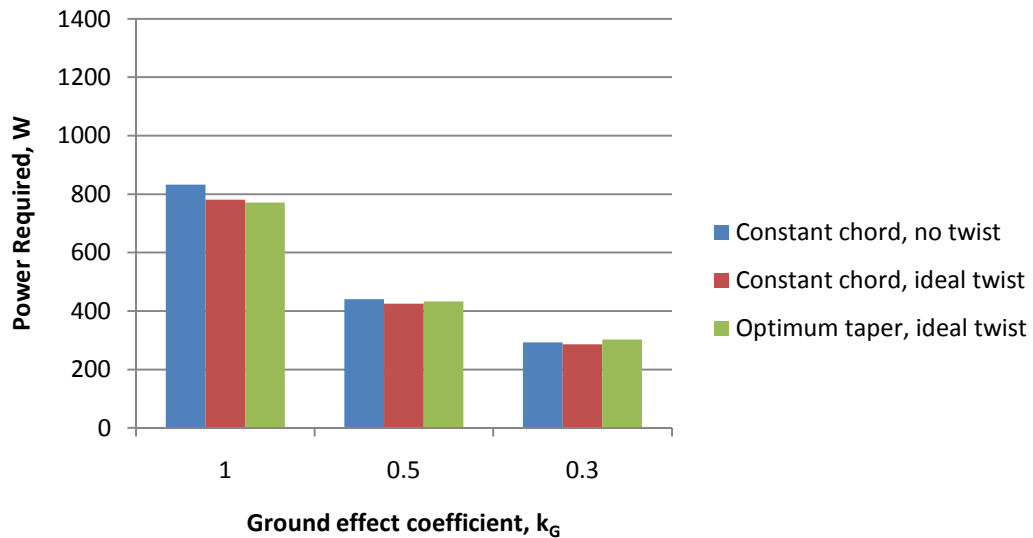
Figure 17: Total power required, R = 75 ft, FX 63-137

These plots give us a very important insight: as the ground effect coefficient decreases, the rotor mode becomes less significant. In fact, in some cases, the optimally designed rotor requires more power than the untapered, untwisted rotor. In addition, we see the enormous impact that the ground effect has on the rotor power required. On average, the power was reduced by 43% when the ground effect coefficient changed from 1 to 0.5,

and decreased another 31% percent when going from 0.5 to 0.3. This equates to an average reduction of 61% when going from 1 to 0.3.

The next series of data helps illustrate why the optimally-tapered rotor does not perform as well as anticipated. Figure 19-22 depict the tip speed at which each rotor achieved its minimum power setting. But first, it should be noted that in some cases, the power required curve would exhibit similar behavior to a drag polar in the sense that for values near the minimum powered required there would be a sort of "power bucket". Figure 18 shows us one example, for the case of the mode 1, 75-foot radius rotor with a NACA 0012 airfoil, which has a minimum power requirement of approximately 533 Watts.
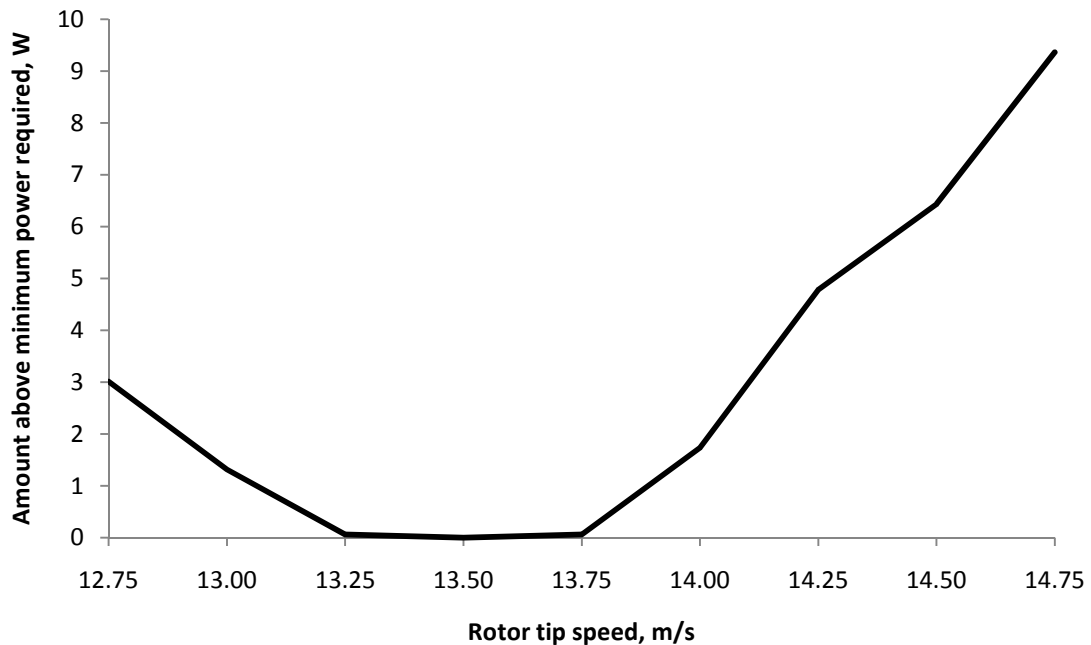
Figure 18: "Power bucket"

We see that there is a range of about ±0.75 m/s where the power is within 5 W of the minimum power point. It could be possible that turning the rotor slightly slower or faster might provide us with benefits that would outweigh the modest power increase. Now let us examine the power-optimal tip speeds for each rotor configuration:
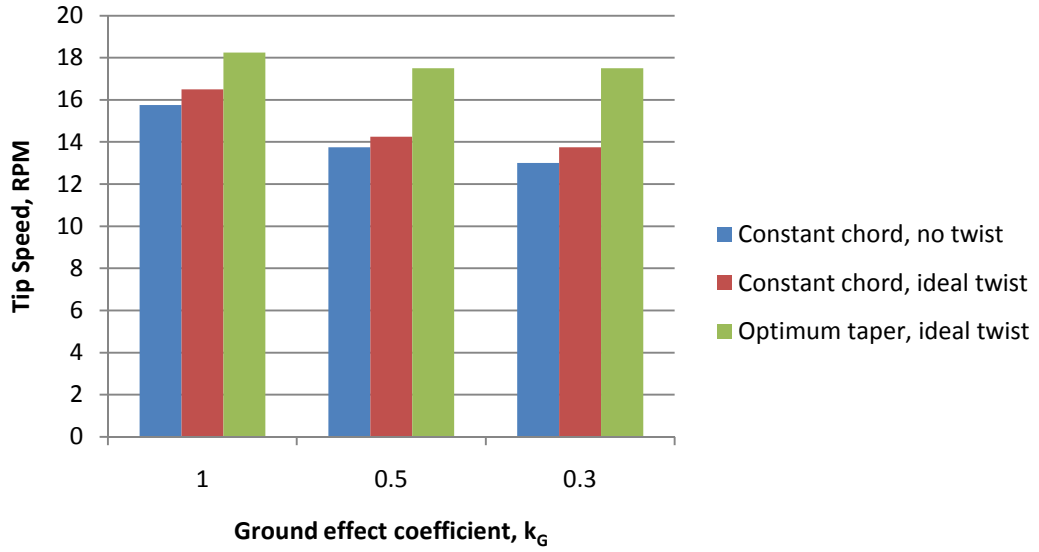
Figure 19: Optimum rotor tip speed, R = 50 ft, NACA 0012
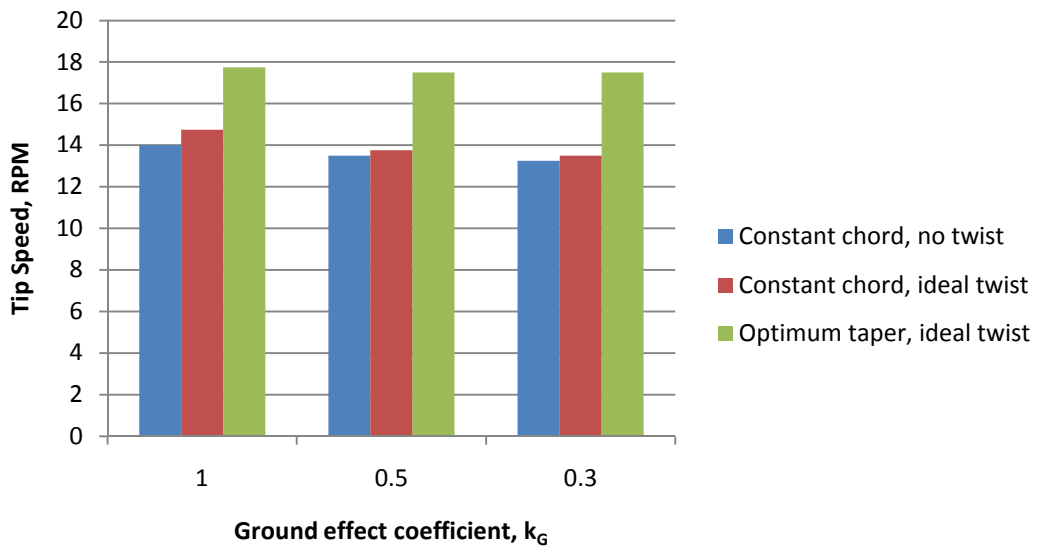
Figure 20: Optimum rotor tip speed, R = 75 ft, NACA 0012
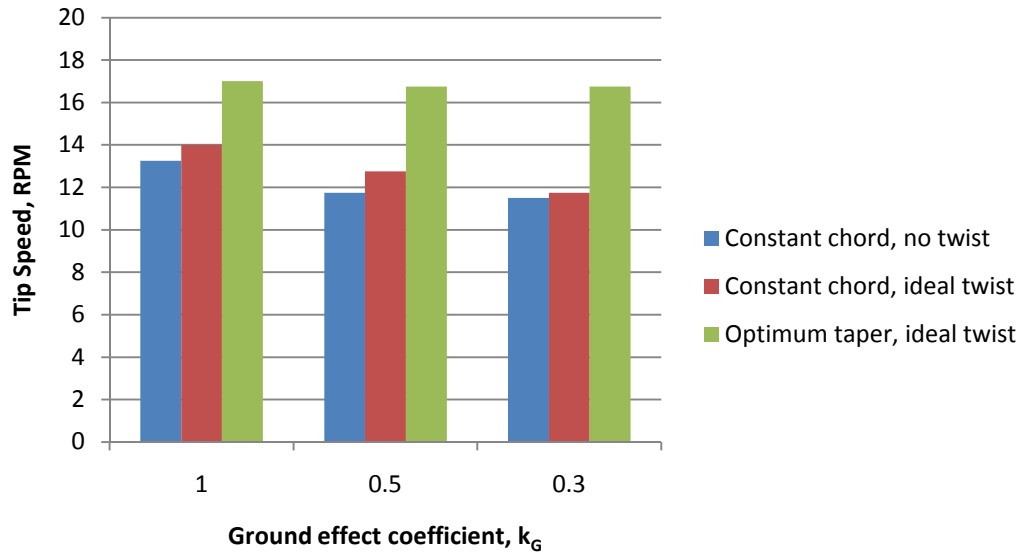
Figure 21: Optimum rotor tip speed, R = 50 ft, FX 63-137
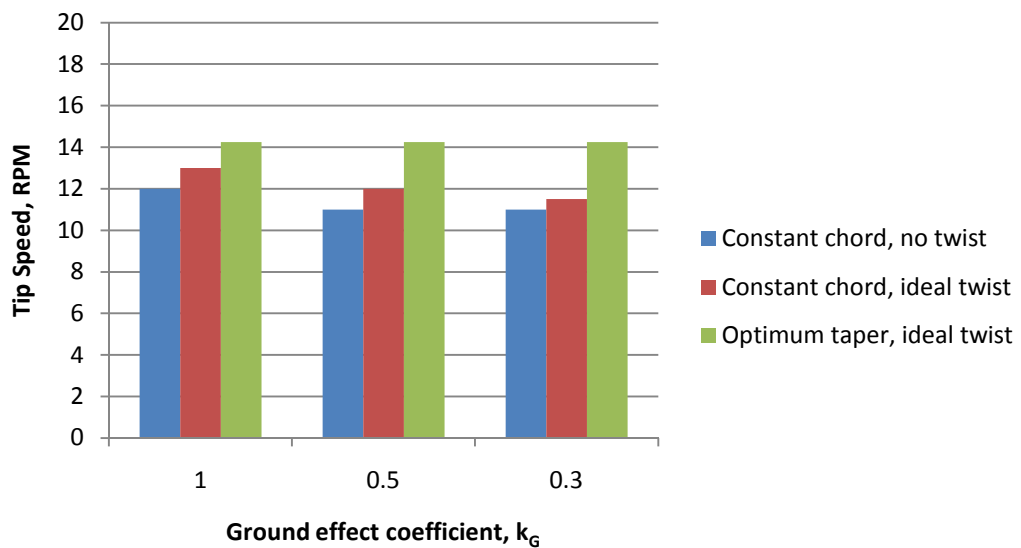
Figure 22: Optimum rotor tip speed, R = 75 ft, FX 63-137

We see for all cases that the optimum tip speed increases considerably when the planform is tapered. This can be attributed to the fact that the local spanwise lift is proportional to the rotor chord. In addition, given that the rotor is designed to yield a triangular lift distribution, the lift forces are greatest at the tips, which is where the chord becomes the smallest when tapered. The first tool used to counter this is an increase in rotor twist,

42

which increases the lift coefficient across the rotor. However, at a certain point the airfoil will reach its maximum lift coefficient, or the drag generated by the additional lift will become excessive. By tapering the chord, the local Reynolds is decreased, which will further degrade the airfoil's lift and drag performance. The likely solution will be for the rotor to turn at a faster speed to achieve maximum performance, as shown in the preceding plots. It should be noted that the optimum tip speed does not fluctuate very much as the ground effect coefficient changes. It is especially stable with the larger radius rotors. The source of this discrepancy between our results and initial predictions can be illuminated further with the following set of plots. Figure 23-26 divide the total power into its induced and profile components. Before we analyze the results, let us recall the simplified equation for power required (repeated from Equation 24):

$$P = \frac{k_G W^{3/2}}{R\sqrt{2\rho\pi}} + W \frac{k_b(\Omega R)}{\frac{\bar{c}_l}{\bar{c}_d}}$$

In comparing these rotors, we held weight and density constant across the entire range, and then compared families of similar ground effect coefficient, radius, blade coefficient, and lift-to-drag performance. We will organize these plots in a different order to emphasize the effects not related to rotor radius, as this will be addressed next.
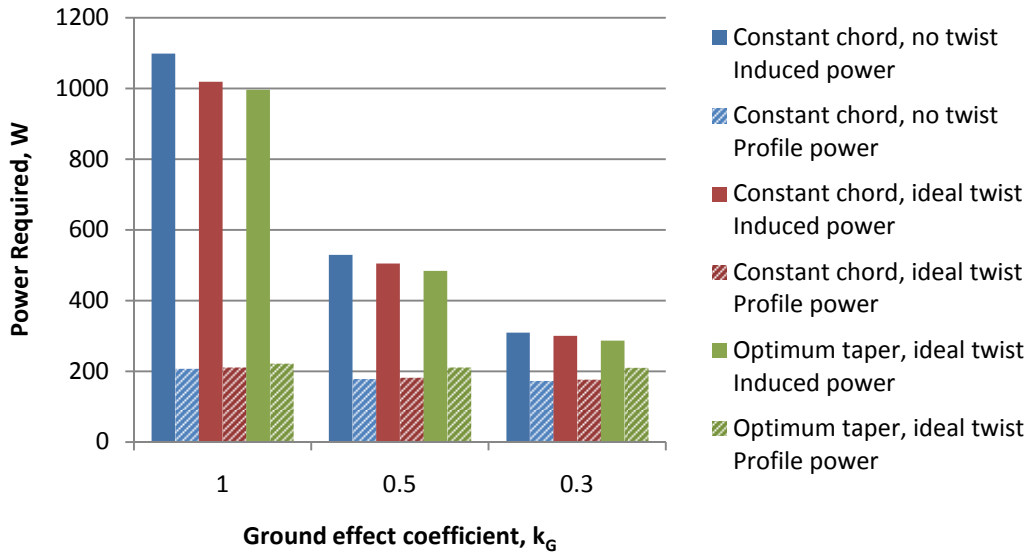
Figure 23: Induced and profile power, R = 50 ft, NACA 0012
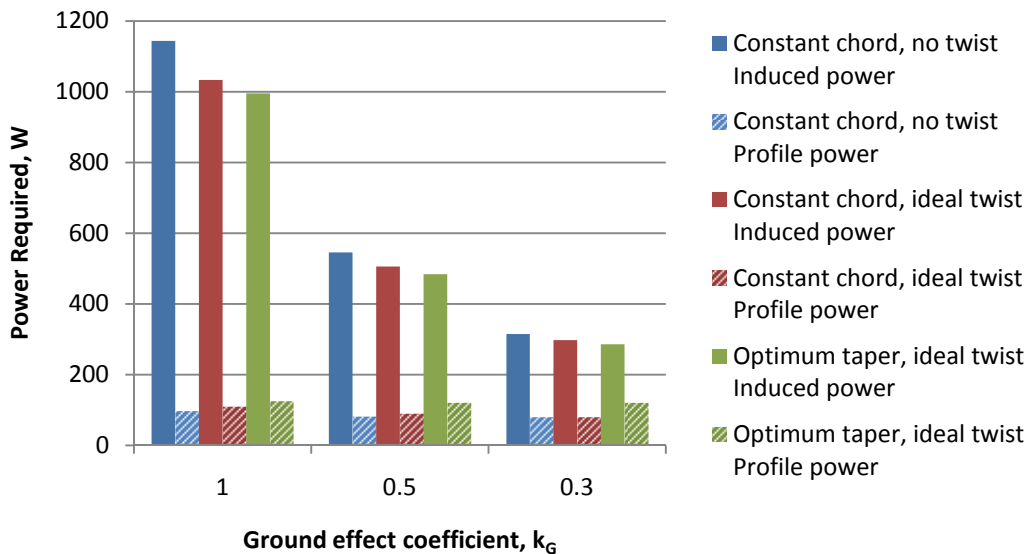
Figure 24: Induced and profile power, R = 50, FX 63-137

We can see that the induced power values are nearly identical for the 50-foot radius

rotors, regardless of airfoil. And just as expected, by utilizing ideal twist, we can reduce

these values a considerable amount. This trend continue for all ground effect coefficients,

although the absolute power benefits from rotor twist are diminished. Notice that the

induced power decreases when the rotor is tapered, even though the twist distributions are similar. As we saw earlier, the optimally tapered rotor achieves it best performance when rotating faster than the constant chord rotor. This will result in a decrease in the inflow velocity ratio, thereby decreasing the twist required to achieve the same angle of attack. This allows for more of the rotor to follow the ideal twist distribution before reaching the specified maximum twist angle.

Looking at the profile power term of Equation 23, we see that the blade coefficient, rotor tip speed, and airfoil performance are all factors that change when the rotor is tapered; the tip speed increases, while the blade coefficient decreases. The airfoil performance will also likely diminish which, as seen in these plots, ultimately results in a profile power increases.
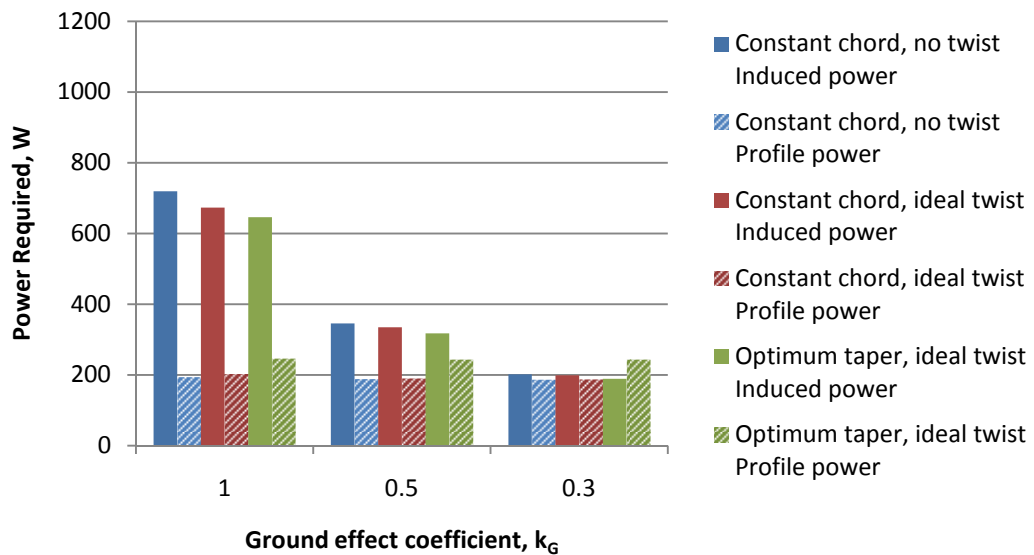
Figure 25: Induced and profile power, R = 75 ft, NACA 0012
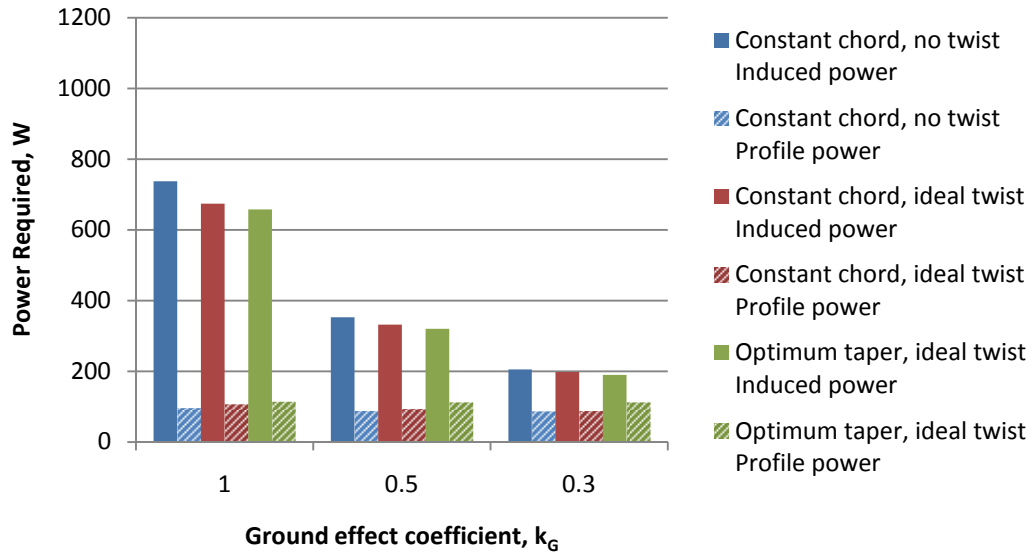
Figure 26: Induced and profile power, R = 75 ft, FX 63-137

The 75-foot radius rotors follow trends similar to that of the 50-foot radius rotors. However we see that the airfoil has even more of an effect on the induced/profile power relationship. Notice that for the NACA 0012 airfoil, when the ground effect coefficient drops to 0.3, the profile power essentially equals (or exceeds) the induced power—a clear distinction from the 50-foot case.

We have visibly identified the effects of all the parameters studied except for the rotor radius. Figure 27-29 will demonstrate the change in power required when increasing the radius from 50 to 75 feet for the NACA 0012 rotor. The FX 63-137 rotor follows a nearly identical trend, so for the sake of brevity only the NACA plots will be included. To infer the radius effect for the FX 63-137 one can simply return to Figure 16 and 17.
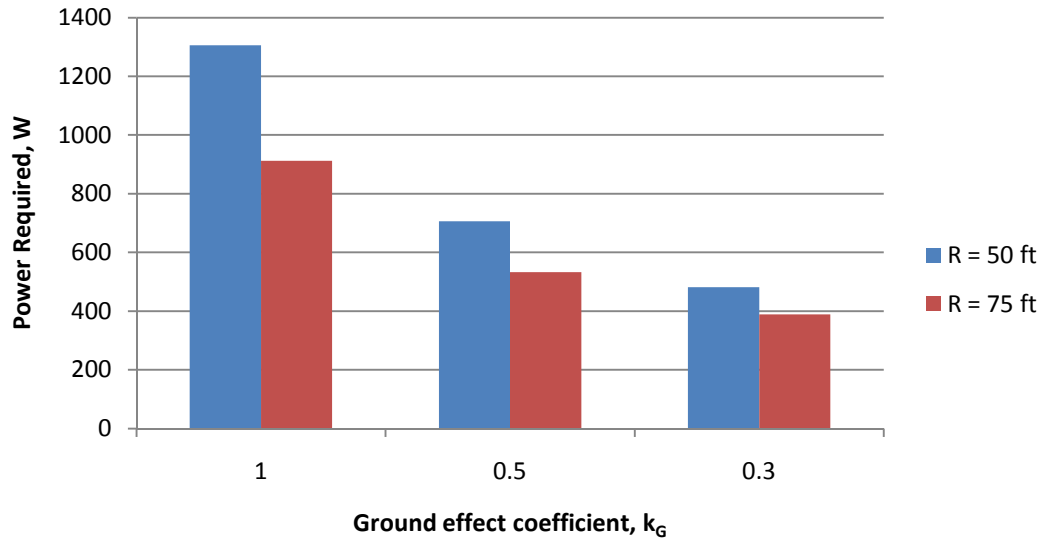
Figure 27: Effect of radius, Constant chord, no twist – NACA 0012
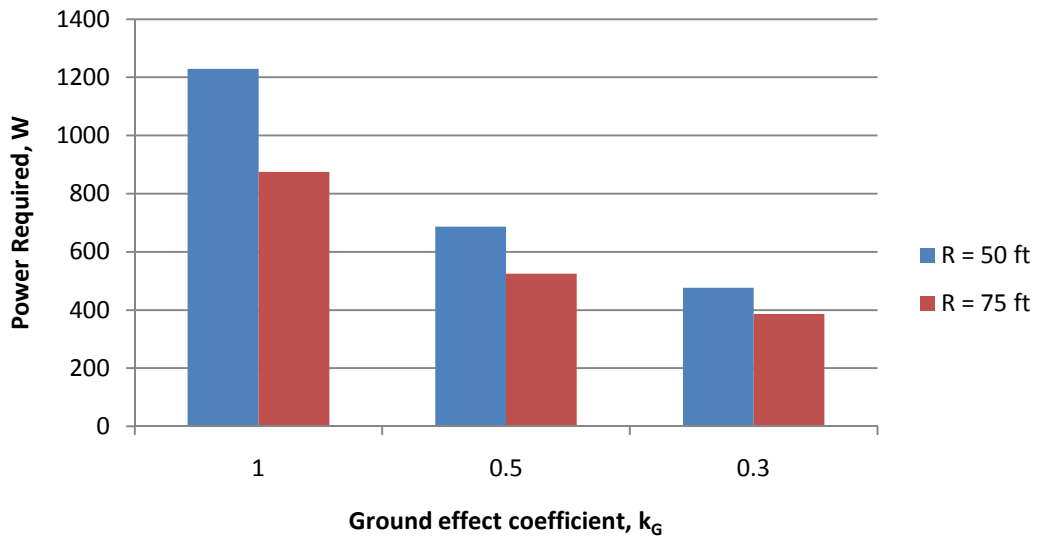
Figure 28: Effect of radius, Constant chord, ideal twist – NACA 0012
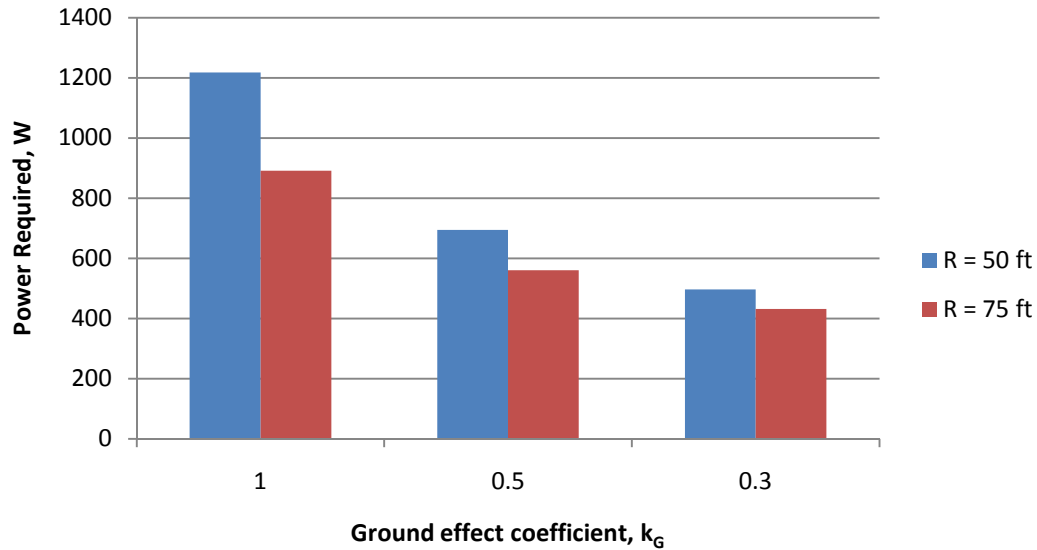
Figure 29: Effect of radius, Optimum taper, optimum twist – NACA 0012

These plots show us one important thing: the effect of the radius decreases along with the ground effect coefficient. For all three configurations the power required drops by approximately 35% when increasing the radius from 50 to 75 feet in the out-of-ground-effect condition. This benefit lowers to 22% with k_G equal to 0.5, and 17% when k_G becomes 0.3. When the rotor is in deep ground effect, the total power required has been already reduced so much that the power savings caused by the radius expansion might not be worth the increase in weight, bending loads, and complexity that would also follow. This leads us to an important conclusion: In order to make effect design decisions, the ground effect coefficient must be known to as accurate a degree as possible.

The consequences of the rotor operating in ground effect are substantial and all-encompassing. The total power required, ratio of induced-to-profile power, and the benefits of a large radius are all significantly affected by this phenomenon. Because all aspects of the design are focused on the balance between aerodynamically-induced power reduction and structurally-induced power reduction, it is paramount that the aerodynamic

tools are extremely accurate. Obtaining a good estimate of the ground effect coefficient is the first step. All subsequent decisions are based on this first assumption, and therefore any errors in its estimation will propagate throughout the design.

Recalling Figure 4, we can add the results of our trade study to get an idea in terms of the power reductions we can expect due to ground effect. Unfortunately we simply specified the ground effect coefficient, so we do not know how our results related to the quantity $/R$, which is what determines the actual magnitude of ground effect. However, for the sake of visualization, Figure 30 incorporates the range of $\frac{P_{IGE}}{P_{OGE}}$ values from the trade study by shading the design space that we might expect for the case of the human-powered helicopter.
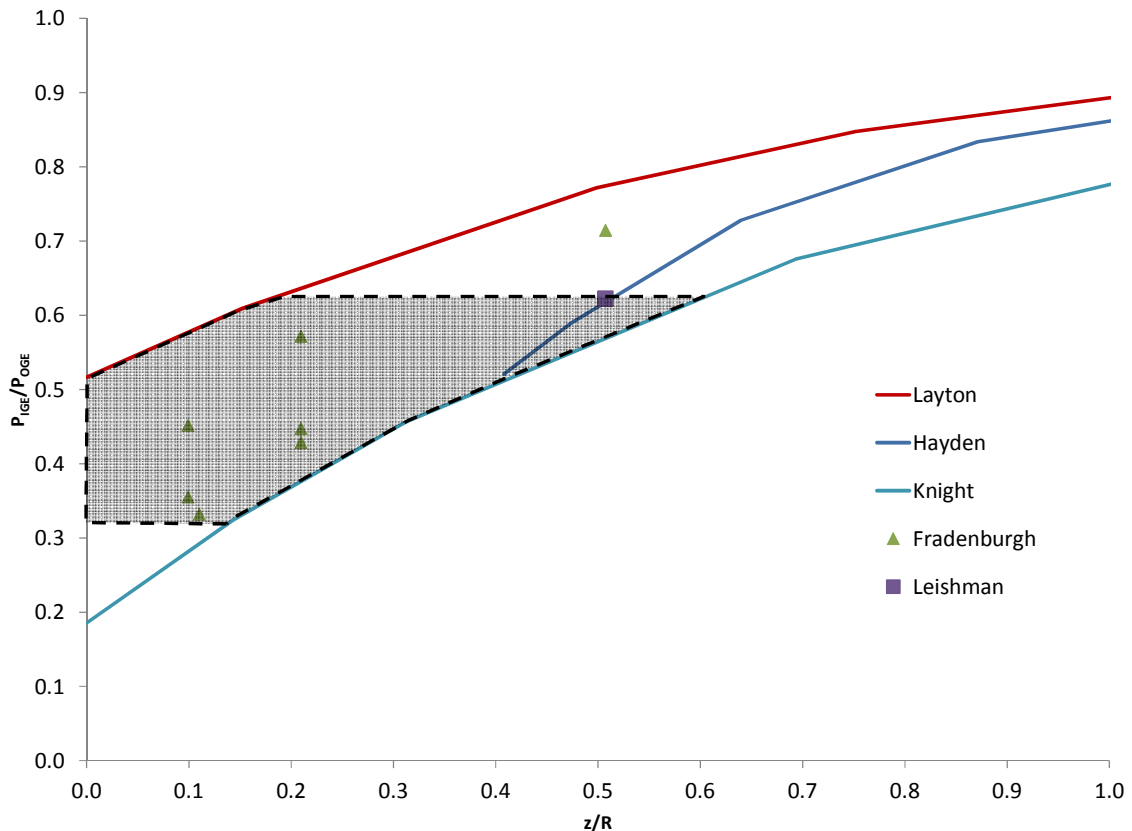
Figure 30: Calculated power reduction due to ground effect

Design Process

Up to this point, our analysis has only included aerodynamic considerations. Obviously

any changes to rotor planform will also affect the structural requirements and

performance of the rotor. For this reason, the design process must link the aerodynamic

and structural aspects. Unfortunately, in order to build accurate structural models, a

certain amount of physical construction and testing must be performed. While there has

been no work done to that end with this project, the places in the design process where

the structural design and analysis will take place have been accounted for. Figure 31

shows the proposed design process in its entirety.
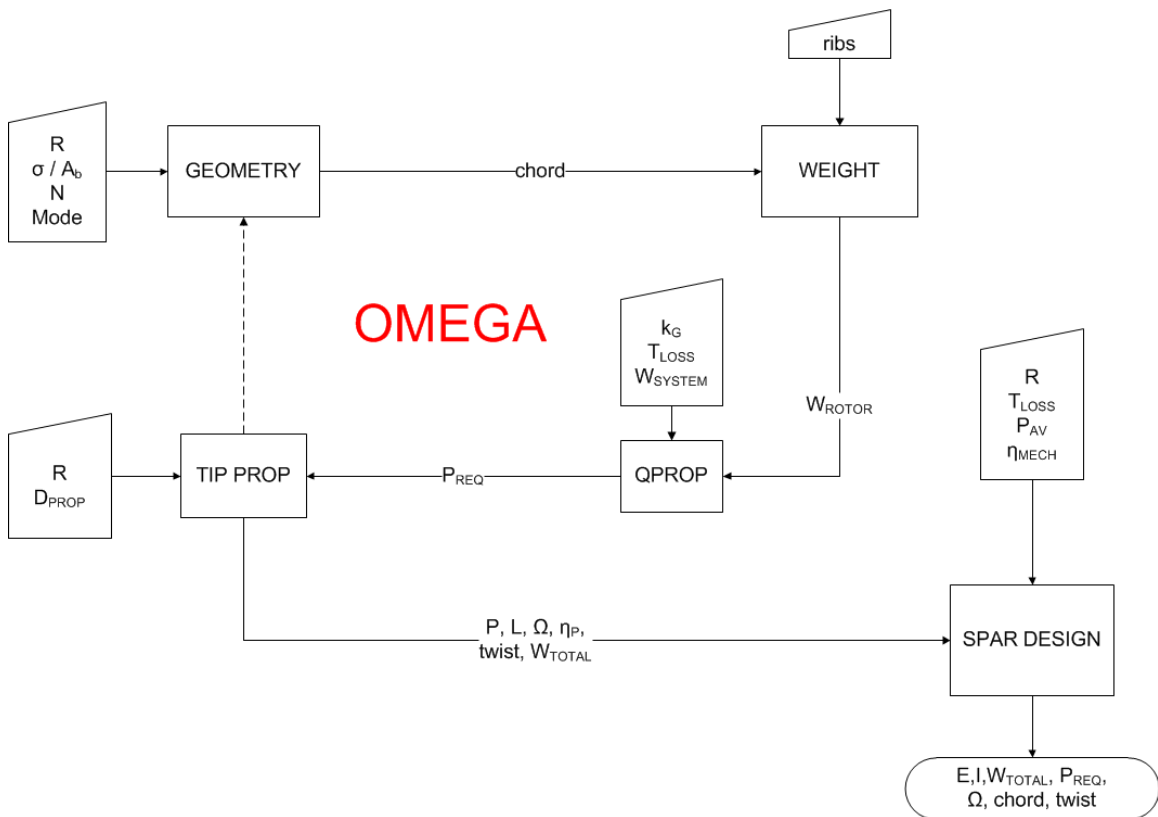
Figure 31: Complete design process

The design loop is intended to have as few inputs as possible. However, given the

number of variables that must be defined in order to have a constrained design, a fair

50

amount of parameters must be set before the process can be executed. This sequence of analysis blocks is not intended to provide a concrete answer, but rather to provide the designer with the necessary data from which to make decisions about the final design. The designer will be able to weigh the consequences of each incremental change, and thus be capable of creating the absolute best helicopter for the given circumstances. While some of these analysis steps are autonomous, others require significant user interaction. Appendix A discusses the inputs for each block, and the ways in which the blocks connect to each other.

Conclusion

The concept of human-powered vertical flight was studied in great depth. Through the manipulation of preexisting theory and analytical methods, a collection of design tools was created to expediently conceptualize and then analyze virtually any rotor. The tools were arranged to form an aerodynamically-focused rotor design process, which can potentially be implemented into a larger complete helicopter design process. We discovered that ground effect is crucial to the design and performance of the helicopter; also essential are the rotor radius and airfoil selection. Every design decision must keep both aerodynamic and structural ramifications in mind. By considering the many aspects of human-powered vertical flight, it appears possible that future engineers can design and build a helicopter capable of capturing the Sikorsky Prize. The preceding discussion should help them get closer to that goal.

Bibliography

Abbott, Ira H. and A. E. von Doenhoff. <u>Theory of Wing Sections</u>. New York: Dover
Publications, 1959.

Ahlin, Gary A. and Richard E. Brown. "Wake Structure and Kinematics in the Vortex
Ring State." <u>Journal of the American Helicopter Society</u> 2009.

Ansley, Les and Patrick Cangley. "Determinants of "optimal" cadence during cycling."
<u>European Journal of Sport Science</u> (2009): 61-85.

Basset, Pierre-Marie, et al. "Prediction of Vortex Ring State Boundary of a Helicopter in
Descending Flight by Simulation." <u>Journal of the American Helicopter Society</u>
2008.

Brown, Richard E. and Glen R. Whitehouse. "Modelling Rotor Wakes in Ground Effect."
<u>Journal of the American Helicopter Society</u> 2004.

Caradonna, F. "Performance Measurement and Wake Characteristics of a Model Rotor in
Axial Flight." <u>Journal of the American Helicopter Society</u> 1999.

Cary, Andrew, Tim Morthland and Eric Loth. "Systems design of the Dragonfly: a
human-powered helicopter." <u>Human Power: Technical Journal of the IHPVA</u>
1995.

Cheeseman, I. C. and W. E. Bennett. "The Effect of the Ground on a Helicopter Rotor in
Forward Flight." Technical Report. Aeronautical Research Council, 1957.

Drela, Mark. "QPROP Formulation." 2006.

Filippone, Antonio. "On the Possibility of Human-Powered Vertical Flight." <u>Journal of
the American Helicopter Society</u> 2007.

Fogelberg, John T. "Da Vinci II Stability Control System." Senior Project 88-0225. 1988.

Fradenburgh, Evan A. "The Helicopter and the Ground Effect Machine." <u>Journal of the
American Helicopter Society</u> 1960.

Fulton, Mark V. and Robert A. Ormiston. "Hover Testing of a Smal-Scale Rotor with
On-Blade Elevons." <u>Journal of the American Helicopter Society</u> 2001.

Griffiths, Daniel A., Shreyas Ananthan and J. Gordon Leishman. "Predictions of Rotor
Performance in Ground Effect Using a Free-Vortex Wake Model." <u>Journal of the
American Helicopter Society</u> 2005.

Group, UIUC Applied Aerodynamics. <u>UIUC Airfoil Coordinates Database</u>. 2010. <http://www.ae.illinois.edu/m-selig/ads/coord_database.html>.

Hepperle, Martin. <u>Propulsion by Propellers</u>. 2005. <http://www.mh-aerotools.de/airfoils/>.

Iboshi, Naohiro, et al. "Ground Effect of a Rotor Hovering above a Confined Area." <u>American Helicopter Society 64th Annual Forum</u>. 2008.

Johnson, Wayne. <u>Helicopter Theory</u>. New York: Dover Publications, Inc, 1980.

Knight, Montgomery and Ralph A. Hefner. "Analysis of Ground Effect on the Lifting Airscrew." Technical Note. 1941.

Knight, Montgomery and Ralph A. Hefner. "Statis Thrust Analysis of the Lifting Airscrew." Technical Note. 1937.

Kogiso, Nozomu and Tatsurou Tsushima. "Wing Planform Optimization of Human Powered Aircraft in Low Reynolds Number Range." 2000.

Lane, Kevin A., David D. Marshall and Rob A. McDonald. "Lift Superposition and Aerodynamic Twist Optimization for Achieving Desired Lift Distributions." (2010).

Langford, John. "The Daedalus Project: A Summary of Lessons Learned." <u>AIAA/AHS/ASEE Aircraft Design, Systems, and Operations Conference</u>. 1989.

Larwood, Scott and Neal Saiki. "Aerodynamic Design of the Cal Poly Da Vinci Human-Powered Helicopter." 1990.

Lissaman, P.B.S. "Wings for Human-Pwered Flight." 1980.

Patterson, William B. "Design process of a Human Powered Helicopter." n.d.

Perry, F. John, et al. "Modeling the Mean Flow through a Rotor in Axial Flight Including Vortex Ring Conditions." <u>Journal of the American Helicopter Society</u> 2007.

"Project: Da Vinci III." n.d. <u>Human Powered Helicopters.</u> <http://www.humanpoweredhelicopters.org/davinci/index.htm>.

"Project: Yuri I." n.d. <u>Human Powered Helicopters.</u> <http://www.humanpoweredhelicopters.org/yuri1/index.htm>.

Prouty, Raymond W. <u>Helicopter Performance, Stability, and Control</u>. Krieger Publishing Company, 2002.

Smith, Justin L., Henry Z. Graham and James E. Smith. "The Validation of an Airfoil in the Ground Effect Regime Using 2-D CFD Analysis." 26th AIAA Aerodynamic Measurement Technology and Ground Testing Conference. 2008.

Standish, K. J. and C. P. van Dam. "Aerodynamic Analysis of Blunt Trailing Edge Airfoils." Journal of Solar Energy Engineering 2003.

Tarascio, Matthew J. "Human Powered Helicopter Competition Guidebook." n.d. <http://www.vtol.org/awards/HPHCBooklet.pdf>.

Thompson, B. E. and R. D. Lotz. "Flow araound a blunt and divergent trailing edge." Experiments in Fluids 2002.

Totah, Joseph J. and William Patterson. "Control of a Human-Powered Helicopter in Hover." Technical Memorandum. 1988.

Wald, Quentin R. The aerodynamics of propellers. Elsevier Ltd., 2006.

Zerweckh, S. H. and A. H. von Flotow. "Flight Testing a Highly Flexible Aircraft; Case Study on the MIT Light Eagle." Department of Aeronautics and Astronautics, Massachusetts Institute of Technology, 1988.

List of References

1. Tarascio, Matthew J. "Human Powered Helicopter Competition Guidebook." n.d. <http://www.vtol.org/awards/HPHCBooklet.pdf>.

2. "Project: Da Vinci III." n.d. Human Powered Helicopters. <http://www.humanpoweredhelicopters.org/davinci/index.htm>.

3. "Project: Yuri I." n.d. Human Powered Helicopters. <http://www.humanpoweredhelicopters.org/yuri1/index.htm>.

4. Johnson, Wayne. Helicopter Theory. New York: Dover Publications, Inc, 1980.

5. Knight, Montgomery and Ralph A. Hefner. "Analysis of Ground Effect on the Lifting Airscrew." Technical Note. 1941.

6. Griffiths, Daniel A., Shreyas Ananthan and J. Gordon Leishman. "Predictions of Rotor Performance in Ground Effect Using a Free-Vortex Wake Model." Journal of the American Helicopter Society 2005.

7. Fradenburgh, Evan A. "The Helicopter and the Ground Effect Machine." Journal of the American Helicopter Society 1960.

8. Hepperle, Martin. Propulsion by Propellers. 2005. <http://www.mh-aerotools.de/airfoils/>.

9. Ansley, Les and Patrick Cangley. "Determinants of "optimal" cadence during cycling." European Journal of Sport Science (2009): 61-85.

10. Drela, Mark. "QPROP Formulation." 2006.

11. Iboshi, Naohiro, et al. "Ground Effect of a Rotor Hovering above a Confined Area." American Helicopter Society 64th Annual Forum. 2008.

12. Larwood, Scott and Neal Saiki. "Aerodynamic Design of the Cal Poly Da Vinci Human-Powered Helicopter." 1990.

13. Abbott, Ira H. and A. E. von Doenhoff. Theory of Wing Sections. New York: Dover Publications, 1959.

14. Group, UIUC Applied Aerodynamics. UIUC Airfoil Coordinates Database. 2010. <http://www.ae.illinois.edu/m-selig/ads/coord_database.html>.

15. Prouty, Raymond W. Helicopter Performance, Stability, and Control. Krieger Publishing Company, 2002.

16. Fogelberg, John T. "Da Vinci II Stability Control System." Senior Project 88-0225. 1988.

17. Lane, Kevin A., David D. Marshall and Rob A. McDonald. "Lift Superposition and Aerodynamic Twist Optimization for Achieving Desired Lift Distributions." (2010).

56

APPENDIX A: Design Process

The design process introduced earlier (reproduced below) will now be discussed in depth.
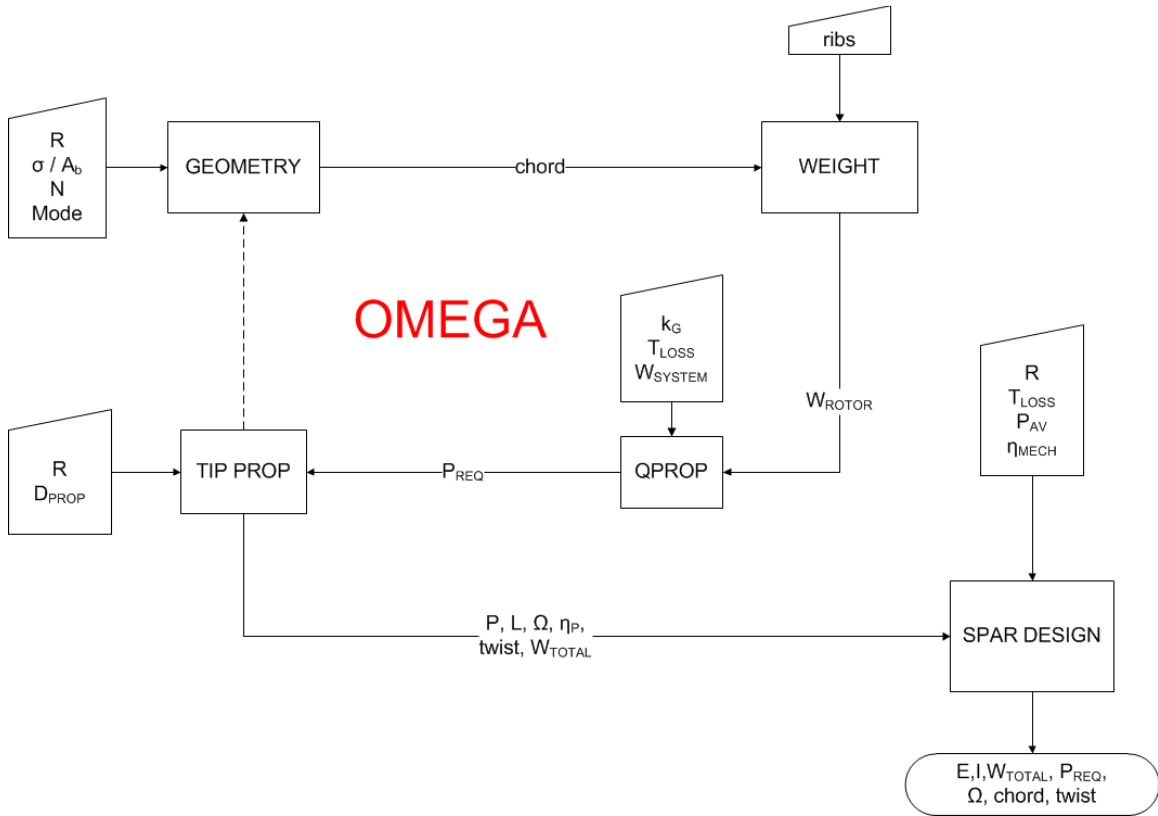
Figure 32: Complete design process (reproduced)

Each block corresponds to one or MATLAB scripts that perform a particular function.

These function, and the inputs and outputs they involve, are explained below.

GEOMETRY

The GEOMETRY block begins the design process and requires four inputs in order to

create an initial rotor planform:

Rotor radius (R): By fixing the radius, we have more of a control on the weight

and strength of the rotor. We can conduct several trade studies in order to see its effects,

but for the iterative process, it should be left as a constant.

57

Rotor solidity (σ) or rotor blade area (A_b): In order to compare rotors, we would like to constrain the rotor blade dimensions somehow, which can most easily be done by fixing the blade area or fixing the solidity. The advantage of the solidity is that it is non-dimensional, which allows it to be relevant for every type of rotor configuration. The advantage of the rotor blade area is that it should theoretically keep the rotor weight from varying as much when the radius is changed. It will also hold the Reynolds numbers constant for corresponding r values.

Number of rotor blades (N): this design study is only considering configurations with two blades. An odd number of blades would create unnecessary complexity at the rotor hub, and any additional blades after four would not provide enough of a benefit to offset their weight. However, the case with four blades should certainly be considered, as it could have potential stability and control benefits.

Mode: In order to create the rotor planform, the mode must be specified beforehand. Many of the differences between modes are qualitative rather than quantitative, and therefore they cannot be compared within an autonomous process.

WEIGHT

The WEIGHT block is crucial to the design process, as it captures the effects of increasing the rotor radius and blade area in terms of weight.

Rib spacing (ribs): In order for the weight to be estimated, a rib distribution must be specified. The other option is to space the ribs so that the critical buckling load or bending moment is the same at each rib. However, this would require some previous knowledge of the rotor spar, which will be designed in a later step. Therefore, at least for

all but the final iterations, the ribs will be spacing according to a predetermined layout, most likely an even spacing, several different evenly-spaced sections placed together, or a linearly-varied spacing.

The WEIGHT block also requires information regarding the construction of the rotor. It uses material densities to determine the weight of the ribs, spars, and skins. The main purpose of this block is to sufficiently incorporate the effects of increasing the rotor radius, chord, and number of ribs, which all lead to structural benefits, but also cause weight increases. The more information that is available about the rotor construction, the higher fidelity output this block will provide. However, if little is known about the rotor at this stage, then the weight function can just assume an area density and evaluate the rotor weight based on this value.

QPROP

With the rotor planform and rotation speed defined, we can now determine the twist necessary to generate enough thrust to hover. This requires five additional inputs:

Ground effects coefficient (k_G)**:** this value will affect the inflow velocity through the rotor, which changes the angle of attack seen along the rotor. Assuming that the rotor placement has been specified, k_G can be estimated according quantity (z/R).

Thrust loss due to coning (T_{LOSS})**:** as the aerodynamic loads increase, the rotor deflects upwards, which changes the direction of the thrust vector. This resultant loss of thrust is treated as a design variable rather than an output because the spar can be strengthened to achieve whatever amount of thrust retention is necessary.

59

Fixed system weight (W_{SYSTEM}): this variable includes all other components of the helicopter that have a fixed weight, such as the pilot, fuselage, rotor hub, and tip propellers. The weights of these components will not likely be known until after construction, so they should be built as early in the design process and possible.

TIP PROP
The tip propellers will be on a scale that is much more common that the main rotor, and therefore their performance will be more predictable. Minimum-induced loss propellers have been researched quite extensively, and have found success on other human-powered vehicles such as the *Daedalus* or *Gossamer*-series human-powered aircraft.

Propeller diameter (D_{PROP}): The primary limiting factor on the performance of the propellers will be their diameter, which is driven by the placement of the rotor (unless the propellers are placed on booms, in which case there is essentially no restriction).

Rotor tip speed (V_{TIP}): If the diameter is known, we can simply design a propeller for maximum efficiency at each of several inflow velocities, which will translate into rotor tip speeds.

Taking the power required output from the QPROP block, we can find the power input necessary to generate enough tip propeller thrust to turn the rotor at the specified rotation speed.

SPAR DESIGN
Once the **OMEGA** loop has finished running and determined a solution for the given inputs, the rotor parameters are then sent to the SPAR DESIGN block. At this point we will know the thrust, power, and weight characteristics of the rotor, how fast it is

spinning, and the resulting spanwise lift distribution. We now have enough information to determine the loads that the spar will see, as well as the power surplus that can be spent on strengthening the spar and implementing a control system. Other than the inputs that have already been discussed, the SPAR DESIGN will need two specified variables:

Pilot power available (P_{AV}): Extensive testing should be done to determine the maximum power output we can expect from the pilot for the duration of the mission.

Total mechanical efficiency (η_{MECH}): this incorporates the total efficiency of the components in between the pilot's feet and the propeller (or rotor) shaft. This value multiplied by the pilot power available will give us the actual value of our available power.

The spar design process is one that will be just as complex as the rotor aerodynamic process, and therefore will not be attempted here. But it is important that the rotor design decisions are made with the spar design in mind. We would like to maximize the volume inside the rotor as best we can, as that will give the spar designer the most room to work with and allow for the spar to be larger and therefore thinner and lighter. The SPAR DESIGN block will output all of the characteristics of the rotor, which can be implemented in the simulation tool described in a later section.

Appendix B: Other Considerations

There are some other factors that may affect the rotor performance that were not researched thoroughly enough to be discussed in depth, but are certainly worth mentioning.

Indoors vs. Outdoors

Da Vinci III was flown inside Cal Poly's Mott Gym. While this building is large enough to seat a couple thousand people, it becomes extremely small when a 100-ft diameter helicopter is placed inside. The amount of air being displaced by the rotors is by no means negligible compared to the size of the room. It was observed that while the *Da Vinci III* rotor blades were spinning, the sports banners hanging on the walls of the gym were sticking out at 90-degree angles. In other words, the air that was being pushed down through the rotor was being circulated out to and up the walls of the gym, hitting the ceiling, and then coming back towards the center of the room. At this point the air would come back through the rotor, so instead of the helicopter operating in a hover condition, it was essentially in a climb. Therefore the rotors were forced to create even more thrust in order to lift off the ground. This phenomenon leads to the belief that when attempting to capture the Sikorsky Prize, the helicopter should be flown out of doors, in as large of an open area as possible.

There is another problem that arises from a room that is too small. Regardless of the operating environment, as the rotor turns, vortices will build at the tips as they gain strength until the point where they are shed from the rotor and head outward in a radial direction. If the rotor was outside, these vortices would simply travel away from the helicopter until they lost their energy and disappeared. However, when inside a room,

they will reflect off the walls and travel back towards the helicopter. They will interact with the rotor blades aperiodically, which will interfere with the stability of the helicopter. Given the fact that the any control inputs will increase the power requirement of the aircraft, these vortices will have a clear adverse effect on its performance. Again, this leads to the argument that the rotor should be operated outside, in extremely still air.

Theory vs. reality

One subject that has not been addressed is the difference between the expected rotor performance and its actual performance. The helicopter rotor blades are designed using very precise methods, and optimized for a very specific condition. In reality, each blade airfoil will not be experiencing the Reynolds number and angle of attack for which it was designed. Assuming that theory used for analysis is sound, this margin of error should hopefully be small, but it will not be negligible. A simple solution would be to just implement a performance degradation factor that would accompany both the lift and drag performance calculations. The other option is to run several analysis cases with the rotor twist at each station being randomly increased or decreased within a given range. This would simulate the uncertainty of the inflow velocity. While the performance factor method seems faster, the designer would be forced to build a physical model for the sake of comparing analytical and experimental results in order to have any faith in the accuracy of the performance factors that are chosen. Therefore the inflow uncertainty method appears to be preferable. However, these are only two suggestions. It is quite likely that another solution exists which would provide better results.

QPROP vs. simple theory

Unfortunately, there is very limited data available for the flight regime in which we are interested. So while we would like to validate the analytical tools we have against some sort of experimental benchmark, we cannot do so for the conditions that the helicopter will experience. One comforting fact is that the theory behind QPROP is relatively simple, meaning that we can analyze the same problems with an elementary code and expect to get similar results. We would be lacking any three-dimensional considerations, but for the most part, our results should agree. There are two ways we can compare these methods:

1. Take the same geometry and analyze it using both methods and then compare performance.
2. Use each method to design a geometry to fulfill the same requirements, and then analyze and compare performance.

The results of the first method appear below for the case of a 75-foot radius rotor, with an FX 63-137 airfoil operating in a regime where the ground effect coefficient is 0.5. The rotor geometry was created to generate 250 lbf of lift when analyzed using QPROP. This same geometry was then analyzed using the simplified theory, which resulted in both thrust and power differences. Because of this, we would also like to look at the differences in power required-per-unit-thrust for each method. Figure 33-35 depict how these two methods vary in their results.
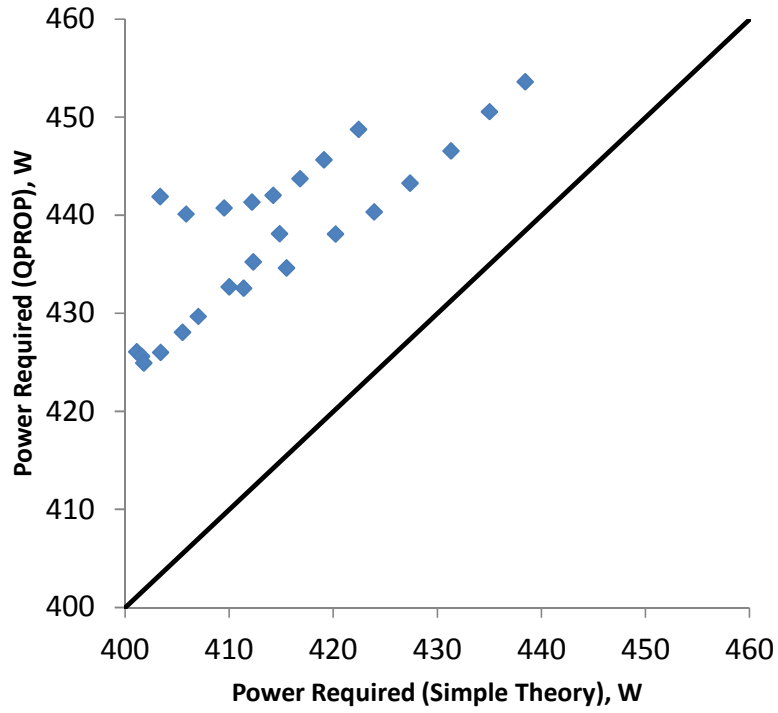
Figure 33: Power comparison
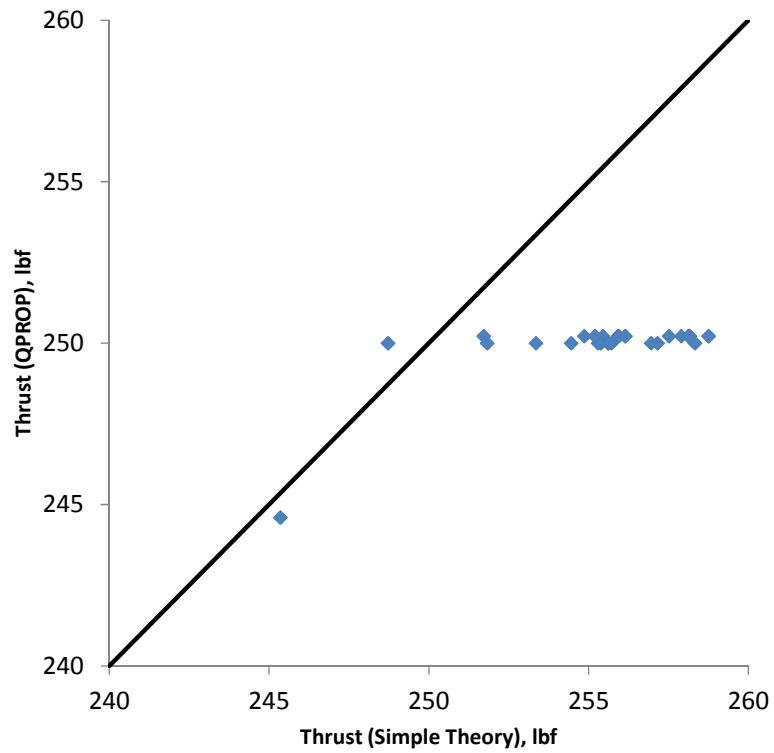
Figure 34: Thrust comparison
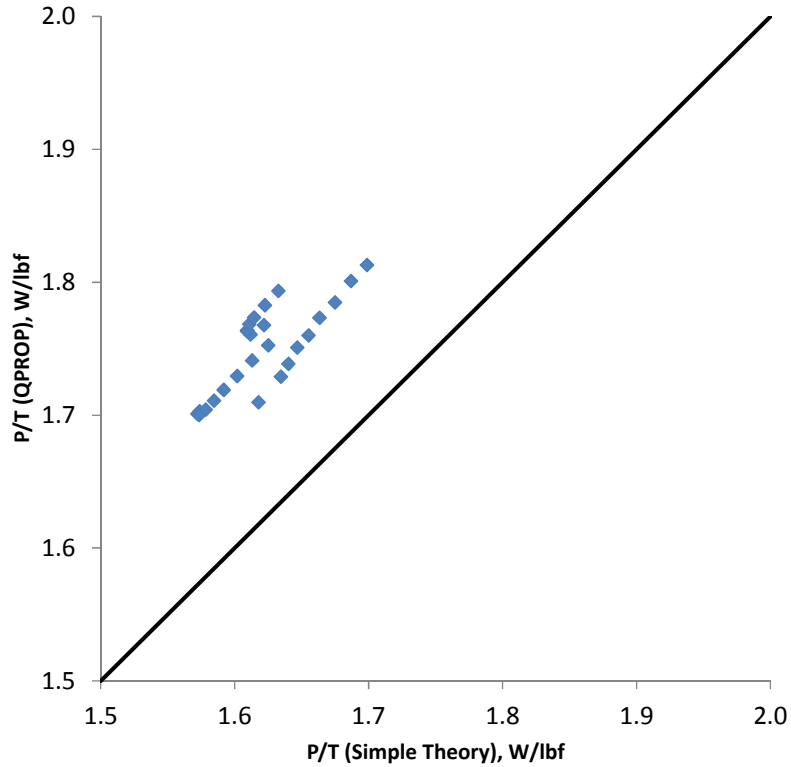
Figure 35: Power-per-thrust comparison

As might be expected, simple theory tends to overestimate the thrust being produced, and underestimate the power required. This can likely be attributed to the tip losses, which QPROP accounts for, but are not addressed with the simply theory analysis. Overall, the results compare well enough that we are confident that QPROP is producing a reasonable solution. Again, this is not considered a rigorous validation, merely a "sanity check".

The second method of comparison was used for all of the analysis done during the trade study. This means that each power value corresponds to a thrust production of 250 lbf. Figure 36-40 show the power comparisons for all configurations analyzed.
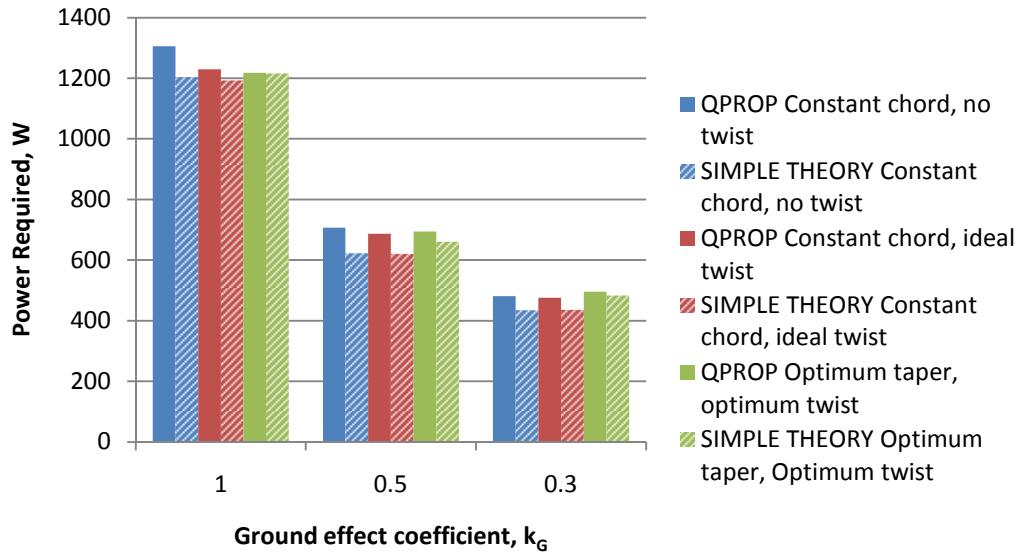
Figure 36: Power comparison, R = 50 ft, NACA 0012
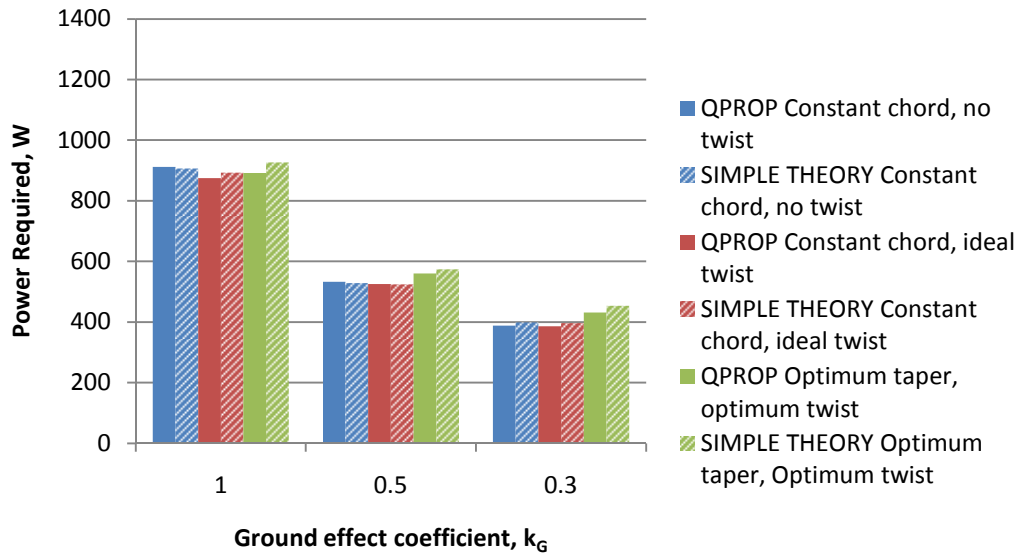
Figure 37: Power comparison, R = 75 ft, NACA 0012
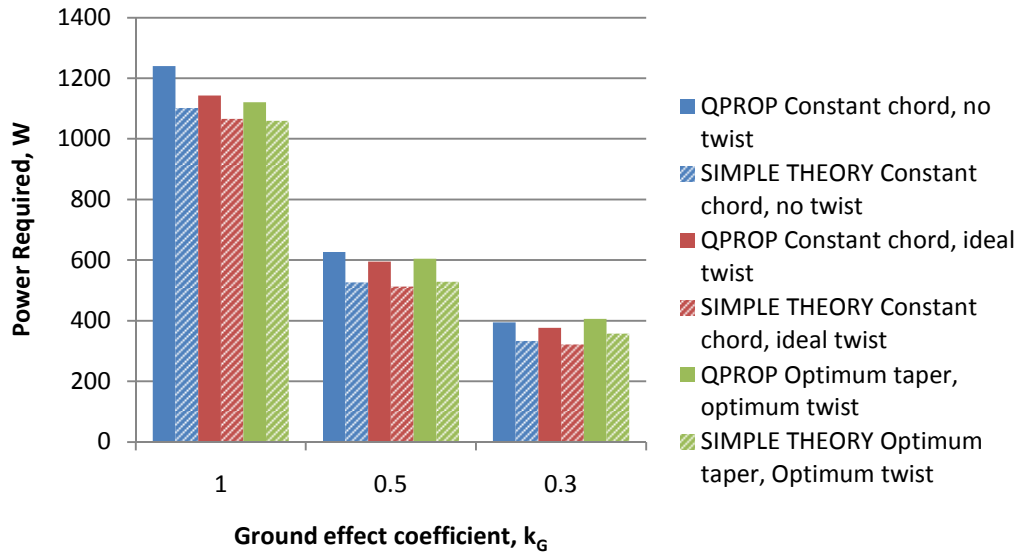
Figure 38: Power comparison, R = 50 ft, FX 63-137
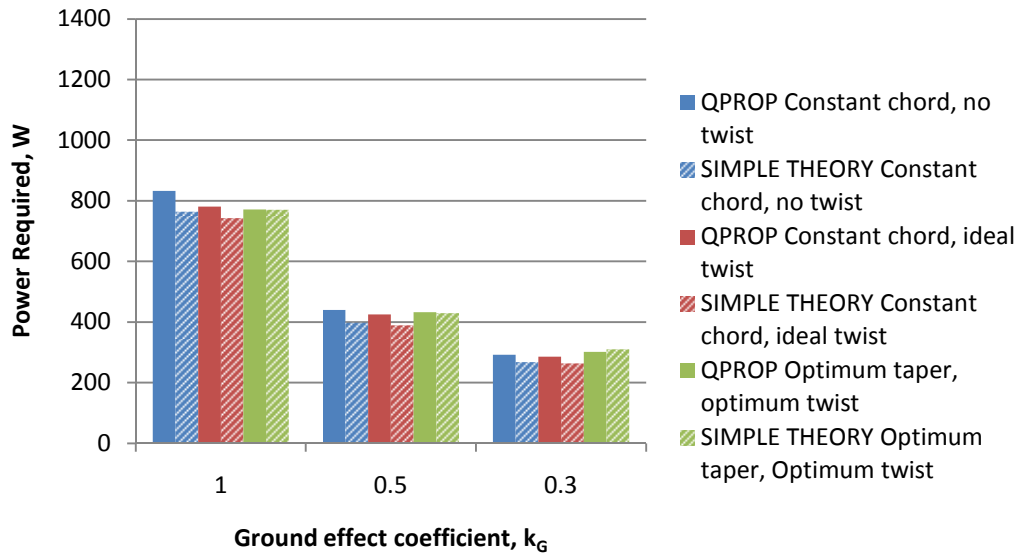
Figure 39: Power comparison, R = 75 ft, FX 63-137
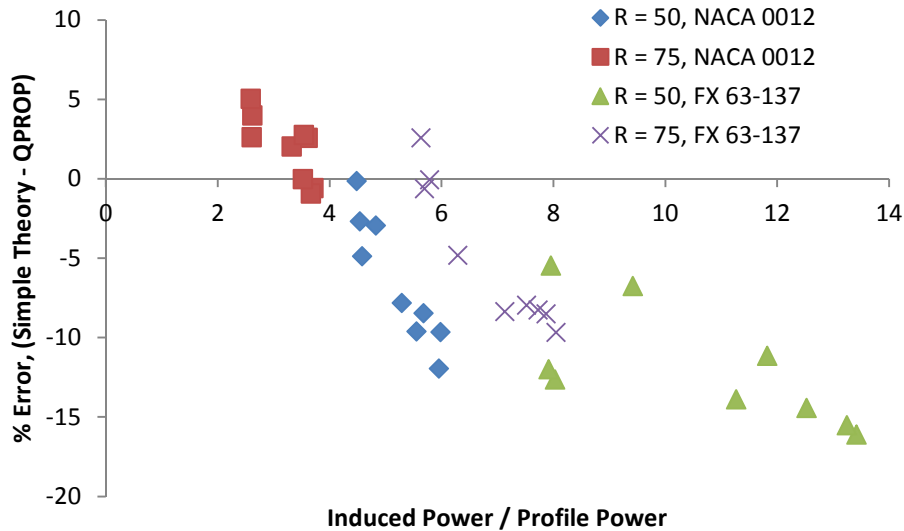
Figure 40: Power ratio effect

We see that QPROP and simply theory yield fairly similar results. Figure 40 points to the leading cause of any differences. As the induced power becomes dominant, the discrepancy between the two methods increases in magnitude, which suggests that the differences in power are tied to the induced power. This matches the earlier-stated presumption that the three-dimensional effects were causing the major discrepancies.

The overall conclusion that can be made from these two comparisons is that QPROP should be used whenever possible, as it is a higher-fidelity solution, which is crucial for the success of this particular problem at hand.

Rotor flapping

The concept of a flapping hinge was developed by the Spaniard Juan de la Cierva in the early 1920's as a remedy to the asymmetrical lift experienced by a rotor in forward flight, which resulted in a strong rolling moment towards the side of the rotor with the retreating blade. By replacing the fixed joint at the rotor hub with essentially a pin joint, the rotor

blade was allowed to move up and down according to the local lift conditions, thereby eliminating the resultant rolling moment. The centrifugal forces acting on the rotor prevented the blades from simply folding up, and instead managed to keep the blades at a reasonable angle of coning. Clearly these asymmetrical loads are not an issue in hover, but the concept of a flapping hinge could still be useful as it would eliminate the moment at the blade root, and could subsequently reduce the structure loads and hence required strength of the blade. It is possible that this weight savings could outweigh the accompanying loss of lift that result from the inherent coning associated with the flapping hinge. To analyze the amount of coning that the rotor would experience, we simply must know the lift distribution across the blade as well as its mass distribution. To quickly discover whether the flapping hinge is even viable, we can make some reasonable simplifications to make the process go very quickly.

First let us examine the lift characteristics of the rotor. The moment caused by the lift at any point r along the rotor can be expressed according to Equation 32, where the first term is the radial station on the rotor, and the second term is the local lift force at the point.

$$M_{LIFT}(r) = r \times L(r)\Delta r \tag{32}$$

To find the moment experience at the blade root, we simply integrate the expression from the root to the tip, as seen in Equation 33.

$$M_{LIFT} = \int_0^R L(r)rdr \tag{33}$$

In terms of the rotor lift, we will assume a triangular lift distribution, which is the theoretically optimum result. If we label the lifting load at the tip L_0 , then the lift distribution can be expressed as Equation 34.

$$L(r) = L_0 \frac{r}{R} \tag{34}$$

Note the fact that the total lift from the two rotors must equal the weight of the helicopter, which we can incorporate into Equation 35.

$$L(r) = W_{TOTAL} \frac{r}{R^2} \tag{35}$$

Putting this result back into Equation 34 and integrating twice, we obtain Equation 36, which provides the moment experienced at the blade root due to the rotor lift.

$$M_{LIFT} = \frac{W_{TOTAL} R}{6} \tag{36}$$

The centrifugal force for an object with mass-per-unit-length m spinning with its center of mass at a distance r from as axis can be expressed by Equation 37, where Ω is the rotation speed in radians/sec.

$$F_{C.F.} = m \Delta r \Omega^2 r \tag{37}$$

This force points outwards away from the axis of rotation, but in the same rotational plane regardless of the coning angle, β. However, the coning of the blade will reduce the moment arm of the force. Assuming the angle is small, this moment arm at a point r along the blade becomes $r\beta$. Therefore the moment at the any point along the blade caused by centrifugal force behaves according to Equation 38.

$$M_{C.F.} = \Omega^2 \beta m r^2 \Delta r \qquad (38)$$

If we assume that the mass is distributed evenly along the blade, we can replace the quantity m with the total mass of the rotor blade, and then solve for the moment seen at the blade root using Equation 39, which clearly becomes Equation 40.

$$M_{C.F.} = \Omega^2 \beta \frac{W_{BLADE}}{gR} \int_0^R r^2 dr \qquad (39)$$

$$M_{C.F.} = \Omega^2 \beta R^2 \frac{W_{BLADE}}{3g} \qquad (40)$$

If the rotor blade is in equilibrium—as it should be while hovering—the moments due to lift and centrifugal forces will be equal, and therefore Equation 41 will be true.

$$R \frac{W_{TOTAL}}{6} = \Omega^2 \beta R^2 \frac{W_{BLADE}}{3g} \qquad (41)$$

For a given rotor design and rotation speed, all of these quantities are known except for the coning angle β, which is solved for in Equation 42.

$$\beta = \frac{W_{TOTAL}}{W_{BLADE}} \frac{g}{2\Omega^2 R} \qquad (43)$$

If we take the *Da Vinci III* as an example, estimating its blade weight at 30 pounds each, with a total weight at 250 pounds, and assuming it would be turning at the design hover rotation speed of 8.5 RPM, we obtain a coning angle of approximately 194°. While this is not likely an accurate result, as the small angle assumption obviously no longer applies, it clearly shows that the rotor is simply not spinning fast enough to the generate the centrifugal force necessary for a flapping hinge to be viable.

Rotor stability

One of the ways in which the stability of the helicopter can be affected is by changing the placement of the rotor itself relative to the center of gravity of the entire craft. *Da Vinci III* was configured with the rotor hub above the rider. This was most likely driven by the ground clearance required for the tip propellers. However, if the propellers were placed on booms in order to raise them up above the rotor, then the rotor plane could essentially be lowered all the way to the ground. For one thing, this would magnify the beneficial effects caused by the ground. It could also conceivably improve the stability of the rotor. A reasonable method for analyzing the behavior of the helicopter as a function of rotor placement begins with first limiting the motion to purely longitudinal movement[16]. The yaw axis is clearly not driving, as there should be essentially zero forces causing any sort heading changes. The lateral behavior should be very similar to the longitudinal result, due to the fact that the helicopter is symmetric about the rotational axis other than the weight distribution of the pilot, which if anything, could be used to help stabilize the aircraft. The longitudinal motion of the helicopter can be defined by Equations 44-46, shown below.

$$-\frac{W_{TOTAL}}{g}\ddot{x} + \frac{\partial X}{\partial \dot{x}}\dot{x} + \frac{\partial X}{\partial \dot{z}}\dot{z} + \frac{\partial X}{\partial q}q - W_{TOTAL}\Theta = -\frac{\partial X}{\partial \theta_0}\theta_0 - \frac{\partial X}{\partial B_1}B_1 \tag{44}$$

$$\frac{\partial Z}{\partial \dot{x}}\dot{x} + \left(\frac{\partial Z}{\partial \ddot{z}} - \frac{W_{TOTAL}}{g}\right)\ddot{z} + \frac{\partial Z}{\partial \dot{z}}\dot{z} + \frac{\partial Z}{\partial q}q = -\frac{\partial Z}{\partial \theta_0}\theta_0 - \frac{\partial Z}{\partial B_1}B_1 \tag{45}$$

$$\frac{\partial M}{\partial \dot{x}}\dot{x} + \frac{\partial M}{\partial \ddot{z}}\ddot{z} + \frac{\partial M}{\partial \dot{z}}\dot{z} - I_{yy}\dot{q} + \frac{\partial M}{\partial q}q = -\frac{\partial M}{\partial \theta_0}\theta_0 - \frac{\partial M}{\partial B_1}B_1 \tag{46}$$

Using the substitutions shown in Equations 47-49, we can alter the equations so that they may be rearranged in order to extract a characteristic equation that will define the

longitudinal motion of the helicopter. The unforced equations in matrix form appear in

Equations 50.

$$x = X(S)e^{st} \tag{47}$$

$$z = Z(S)e^{st} \tag{48}$$

$$\Theta = \Theta(S)e^{st} \tag{49}$$

$$
\begin{bmatrix}
\left(-\dfrac{W_{TOTAL}}{g}s + \dfrac{\partial X}{\partial \dot{x}}\right) & \dfrac{\partial X}{\partial \dot{z}} & \left(\dfrac{\partial X}{\partial q}s - W_{TOTAL}\right) \\[2ex]
\dfrac{\partial Z}{\partial \dot{x}} & \left(\left[\dfrac{\partial Z}{\partial \ddot{z}} - \dfrac{W_{TOTAL}}{g}\right]s + \dfrac{\partial Z}{\partial \dot{z}}\right) & \dfrac{\partial Z}{\partial q}s \\[2ex]
\dfrac{\partial M}{\partial \dot{x}} & \left(\dfrac{\partial M}{\partial \ddot{z}}s + \dfrac{\partial M}{\partial \dot{z}}\right) & \left(-I_{yy}s^2 + \dfrac{\partial M}{\partial q}s\right)
\end{bmatrix}
\begin{bmatrix}
\dot{x}(S) \\[2ex]
\dot{z}(S) \\[2ex]
\Theta(S)
\end{bmatrix} = 0 \tag{50}
$$

After several cancellations, which are not presented here, the characteristic equation

obtained by expanding the determinant appears in Equation 51.

$$
s^4 - \left[\frac{g}{W_{TOTAL}}\left(\frac{\partial X}{\partial \dot{x}} + \frac{\partial Z}{\partial \dot{z}}\right) + \frac{1}{I_{yy}}\frac{\partial M}{\partial q}\right]s^3 + \frac{\partial Z}{\partial \dot{z}}\left[\left(\frac{g}{W_{TOTAL}}\right)^2\frac{\partial X}{\partial \dot{x}} + \frac{g}{W_{TOTAL}I_{yy}}\frac{\partial M}{\partial q}\right]s^2 + \frac{g}{I_{yy}}\frac{\partial M}{\partial \dot{x}}s -
$$

$$
\frac{g}{W_{TOTAL}I_{yy}}\frac{\partial M}{\partial \dot{x}}\frac{\partial Z}{\partial \dot{z}} = 0 \tag{51}
$$

While we can use this equation, it might be more useful to make one additional

simplification in order to reduce the characteristic equation from its fourth-order form to

that of a third-order. By constraining the helicopter in the Z-direction (as would be

appropriate for hover), we can reduce the number of state variables by one, resulting in

Equations 52 and 53.

$$-\frac{W_{TOTAL}}{g}\ddot{x} + \frac{\partial X}{\partial \dot{x}}\dot{x} + \frac{\partial X}{\partial q}q - W_{TOTAL}\Theta = -\frac{\partial X}{\partial B_1}B_1 \tag{52}$$

$$\frac{\partial M}{\partial \dot{x}}\dot{x} - I_{yy}\dot{q} + \frac{\partial M}{\partial q}q = -\frac{\partial M}{\partial B_1}B_1 \tag{53}$$

Using the same substitutions as defined previously, we can again put the unforced version

of these equations in matrix form.

$$\left[\begin{matrix} \left(-\frac{W_{TOTAL}}{g} s + \frac{\partial X}{\partial \dot{x}} \right) & \left(\frac{\partial X}{\partial q} s - W_{TOTAL} \right) \\ \frac{\partial M}{\partial \dot{x}} & \left(-I_{yy} s^2 + \frac{\partial M}{\partial q} s \right) \end{matrix} \right] \left[\begin{matrix} \dot{x}(S) \\ \Theta(S) \end{matrix} \right] = 0 \tag{54}$$

Taking the determinant of the square matrix, we obtain the characteristic equation of the

longitudinal motion.

$$s^3 - \left(\frac{g}{W_{TOTAL}} \frac{\partial X}{\partial \dot{x}} + \frac{1}{I_{yy}} \frac{\partial M}{\partial q} \right) s^2 + \frac{g}{I_{yy}} \frac{\partial M}{\partial \dot{x}} = 0 \tag{55}$$

While we could find the roots of this equation, it would be easier to analyze the effects of

the rotor placement by simply determining the coefficients. Appearing in the form of

Equation 56 shown below, Equation 55 can be used to calculate Routh's discriminant,

which can predict whether the rotor will be unstable, neutrally stable, or stable.

$$As^3 + Bs^2 + Cs + D = 0 \tag{56}$$

Routh's discriminant for a cubic function is defined by Equation 57, which in this case

becomes Equation 58.

$$R.D. = BC - AD \tag{57}$$

$$R.D. = - \left(\frac{g}{I_{yy}} \frac{\partial M}{\partial \dot{x}} \right) \tag{58}$$

We are purely interested in the sign of this value, and the term $\frac{g}{I_{yy}}$ clearly will be positive.

Therefore we must only evaluate $\frac{\partial M}{\partial \dot{x}}$ and we will obtain some important information

about the inherent stability of the helicopter. Equation 59 shows how this term can be found.

$$\frac{\partial M}{\partial \dot{x}} = \frac{dM}{da_{1_S}} \frac{\partial a_{1_S}}{\partial \mu} \frac{\partial \mu}{\partial \dot{x}} - \left(\frac{\partial X}{\partial \dot{x}}\right) h_M \qquad (59)$$

Because the stability derivatives that appear in this equation require some general knowledge about the helicopter, we will use *Da Vinci III* as an example. However, rather than using the tapered rotor of *Da Vinci III*, a constant-chord rotor with the same radius and solidity will be utilized. The calculations for this analysis appear in Appendix D, however the conclusion from this analysis appears below.

$$h_M < -0.90 \ in \longrightarrow \frac{\partial M}{\partial \dot{x}} < 0 \qquad (60)$$

We look to Table 4 and see that if *Da Vinci III* were to be placed at least 0.9 inches below the helicopter's center of gravity, Routh's discriminant becomes negative, which implies that the rotor will not exhibit any unstable oscillation. Placed directly at 0.9 inches below the center of gravity, the helicopter should be neutrally stable. Anywhere above that and the helicopter becomes unstable.

Table 4: Routh's discriminant

TEST	CONSEQUENCE
1. All coefficients are positive	No pure divergence
2. R.D. is positive	No unstable oscillation
3. R.D. = 0	Neutrally stable
4. R.D. is negative	Unstable
5. D = 0 (for cubic, E = 0 for quartic)	Non-oscillatory
6. One coefficient is negative	Pure divergence or unstable oscillation

We now have the coefficients A and D from Equation 55, and C is clearly zero. Solving for B will allow us to determine if the helicopter might exhibit any pure divergence.

$$B = \frac{g}{W_{TOTAL}} \frac{\partial X}{\partial \dot{x}} + \frac{1}{I_{yy}} \frac{\partial M}{\partial q} \tag{61}$$

$$B = \left[\frac{16\rho A_b (\Omega R)^2}{\gamma \Omega \left(1 - \frac{e}{R}\right)^2} \right] \left\{ \begin{array}{l} \frac{g}{W_{TOTAL}} \left[\frac{3}{2} \left(C_T/\sigma - \frac{a}{18} \theta_{.75} \right) \right] \left(\frac{1}{\Omega R} \right) - \\ \frac{1}{I_{yy}} \left[\frac{\frac{3}{4} ea}{\gamma} + \frac{3}{2} \left(C_T/\sigma - \frac{a}{18} \theta_{.75} \right) h_M \right] \end{array} \right\} \tag{62}$$

$$B = k_1 (k_2 - k_3 - k_4 h_M) \tag{63}$$

We see that depending on the positive constants k_1, k_2, k_3, and k_4, as well as the sign

and magnitude of h_M, the coefficient B could either be positive or negative. However, we

expect B to be negative (see Appendix D), which according to Table 4 will result in a

pure divergence, represented by the helicopter's tendency to translate across the ground

during flight. In other words, given the best case scenario, the aircraft will still require

some sort of control system, although placing the rotor beneath the pilot will likely ease

the requirements of the system considerably.

This method has a limitation in the fact that the reactions of the rotor to any perturbations

will occur more slowly than with a typical helicopter rotor spinning at a much higher

rotation speed. More work is necessary to determine just exactly what part of the theory

can be applied to the human-powered helicopter application. There are two senior

projects in the Kennedy Library archives at Cal Poly that discuss this issue in reference to

designing a control system for the *Da Vinci* series of helicopters. Since controllability is a

major issue in terms of staying with a 10-meter box for the Sikorsky Prize, this issue

should be investigated more closely in the future.

Rotor Wind-up Simulation

One factor that not been discussed in other reports is the significance of the wind-up

portion of the helicopter mission. The vigor and duration of the output required during

the time from when the rotor is at rest until it has reached the rotation speed required for

hover has the potential to affect the pilot's energy available for the remainder of the flight

(this is most relevant when the rotor is driven by tip propellers, as there is not a single

direct physical link between the output of the rider and the rotation of the rotor, but rather

additional connections of the rider to the propeller, and the propeller to the air). With the

human pilot already on the cusp of his/her performance threshold, the path taken to reach

the hover rotation speed could possibly make the difference between a successful and

unsuccessful mission.

There are two parts to the design and analysis of the wind-up procedure: the design of the

rotor, and the pilot output "schedule".

To understand how the rotor design affects the rotor wind-up, we can employ the

relationship between torque and angular acceleration, as seen in Equation 64.

$$\alpha = \frac{\tau}{I} \tag{64}$$

To put this in a more familiar format, let us use the following definition of torque.

$$\tau = \frac{P}{\Omega} \tag{65}$$

Substituting this back into Equation 64, we obtain Equation 66.

$$\alpha = \frac{P}{I\Omega} \tag{66}$$

Note that the power in this equation is the net power applied to the rotor shaft, which can be expressed as the difference between the power supplied by the rider (multiplied by the total system efficiency) and the power required to spin the rotor at the current rotation speed.

$$\alpha = \frac{P_{rider}\eta_{total} - P_{rotor}}{I\Omega} \tag{67}$$

The larger the angular acceleration, the less time the pilot has to be pedaling during the wind-up phase, which will leave him/her with more energy for the hover and climb portions of the flight. Clearly designing the rotor to turn with a minimum power requirement will produce higher accelerations, but this has been a driving factor from the beginning. We turn instead to the denominator, which holds the rotor angular moment of inertia I, as well as the rotation speed, Ω. By making a conscious effort to keep the mass of the rotor concentrated as much towards the rotor shaft as possible, the moment of inertia will be minimized. Building the aircraft as light as possible is not the only means by which this is accomplished. One must also consider the inertial impacts of each planform design. A tapered chord will place less mass towards the tip of the rotor, which may offset the manufacturing penalty by increasing the wind-up performance.

Pilot output

It has been repeatedly demonstrated that a human can deliver low power outputs for hours at a time. At a certain point however—which varies from individual to individual—the strain on the body transitions from being purely aerobic to purely anaerobic. Humans can maintain anaerobic activity for much shorter periods of time. As the power demand increases, the sustainable duration decreases respectively. While this is an intuitive

concept, it is very difficult to predict the possible duration for any given output level. Instead, one must rely primarily on testing to determine the performance capabilities of the pilot. This adds a level of difficulty when it comes to designing the rotor, as one must first know the rotor power requirements before a suitable testing and training program can be developed and implemented. At the same time, if the capabilities of the pilot were thoroughly determined beforehand, the data could be used to positively influence the rotor design.

Rather than attempt to determine the power requirements before the rotor has been designed, we can simply determine the most efficient way for the rotor to wind-up. A simulation was created using MATLAB's *ode45* function, which can numerically evaluate a given set of ordinary differential equations. In this case the equations for angular acceleration and angular velocity were used. When written with respect to time, they can be presented according to the following equations.

$$\frac{d^2\theta}{dt^2} = \frac{\tau}{I} \tag{68}$$

$$\frac{d\theta}{dt} = \Omega \tag{69}$$

The simulation begins with the rotor at rest and runs until it has reached hover rotation speed. At each time step the function evaluates each parameter. As discussed earlier, the torque is a function of the rotor power required and the power output by the pilot seen at the rotor shaft. Because the pilot is driving propellers at the tip of the rotor, this power output will vary with rotor rotation speed as well as pilot power input.

In the past, the pilot would begin by pedaling as hard as possible, and continue this effort throughout the duration of the flight. However it might be possible to experiment with different power "schedules" to keep the pilot's effort in the aerobic range for as long as possible. The only foreseeable downside is that a longer run time would require a larger supply of thread to be wound around the tip propeller shafts. This could add to the probability of the thread getting tangled while the propellers were being driven, and also conceivably contribute a non-negligible increase in system weight and moment of inertia. Nevertheless, the prospect of reducing the pilot load significantly is certainly worth the effort of developing this simulation to a level of high fidelity. The tools to predict the rotor power required and tip propeller output are already in place, and measuring the total efficiency between the rider and propeller would be a simple task. The tedious part of the simulation development would be weighing each component of the rotor so that an accurate estimation of the moment of inertia can be obtained. With these elements in place, the simulation can be run as many times as necessary, with a very low computational cost to the user.

The concept of the ideal path to 3 meters raises another issue to consider: off-design performance.

Off-design performance
One unfortunate fact about the Sikorsky Prize task is that the rotor must be capable of operating within a 3-meter range in terms of height above the ground. We have already seen the significance of ground effect, and how it—and the corresponding rotor design— varies with z/R. We must select the ground effect coefficient at the very beginning of the design process. For example, if we would like the rotor to be most efficient at a height of

3 meters, then it will be at an off-design condition for the entire climb up to 3 meters. This would not likely be ideal, as we would rather spend as little time at 3 meters as possible. Thus, there are two quantities that must be balanced: time spent hovering, and time spent climbing. The fact that our pilot is human makes this problem all the more difficult. In purely mathematical terms, it is ideal to spend as little time climbing as possible; this results in the least amount energy being expended. However, this may require such a large power output from the pilot that their available power degrades much more quickly than would otherwise occur with a modest output. And so we must balance the benefits of the power reduction in deeper ground effect with the potential reduction in pilot workload by allowing more time for the climb. Again, this all depends on physiology, and so much more research is needed before a conclusion can be reached.

Appendix C: Methods

There were several methods mentioned in the body of this paper whose details were not shown. The section will portray the details behind those methods, which should allow the reader to reproduce the same conclusions, if desired.

Linear algebra method for desired inflow or lift distribution

A method for achieving an arbitrary lift distribution with an arbitrary wing planform was developed by a student and two professors at Cal Poly[17]. This concept was applied to a helicopter rotor with the expectation that similar principles would apply, thereby allowing an arbitrary inflow velocity distribution to be generated with an arbitrary rotor planform. Assuming that the airfoil is known for every radial location on the blade, the velocity distribution is achieved by altering the twist on the blade. For this particular application, we were only interested in a uniform velocity distribution, as this is the condition required for a minimum-power rotor. However, this method was also used to generate arbitrary lift distributions over the rotor.

The governing principle behind this method is a simple application of linear algebra, utilizing the well-known form of Equation 70.

$$A \cdot \vec{x} = \vec{b} \tag{70}$$

Using our analytical tools we can build the A matrix and $\vec{b}$ vector, so that we may solve for the $\vec{x}$ vector, which will be the incremental incidence that must be added to the current rotor incidence in order to obtain the desired inflow velocity distribution. The defining dimension of these matrices is N, which is equal to $\frac{n+1}{2}$, where n is the number of radial stations (and always odd). While the effects of each radial station was analyzed,

only every other station was used to build the A matrix in order to reduce the singularity that tended to accompany the use of too many entries.

$$\vec{x} = \begin{bmatrix} \theta_1 \\ \theta_2 \\ \vdots \\ \theta_N \end{bmatrix} \qquad (71)$$

The first step in the process was to evaluate a given rotor at the design conditions, but with zero degrees incidence. The results from this analysis were set as the baseline condition. The rotor was also evaluated at the design condition, which was created using blade element and moment theory. By subtracting the baseline results from the design results, we were able to build the $\vec{b}$ vector as seen in Equation 72, with each entry corresponding to one of the N cases.

$$\vec{b} = \begin{bmatrix} v_{1,desired} - v_{1,baseline} \\ v_{2,desired} - v_{2,baseline} \\ \vdots \\ v_{N,desired} - v_{N,baseline} \end{bmatrix} \qquad (72)$$

Then N cases were run, with the index i having an initial value of 1, and incrementing by 2 at each iteration. At each case the incidence at the ith radial station (θ_i) was set to 1°, and the radial stations on either side (θ_{i-1}, θ_{i+1}) were set to 0.5° (except of course at the boundaries, where only there was only one point within the range of the rotor). All the other radial stations retained their zero-incidence settings. This was done so that the effect of each radial stations on the inflow velocity could be determined, thereby allowing the theory of superposition to be utilized in building a twist distribution to match the desired inflow velocity distribution. With each case, a row was added to the A matrix. Because the analysis yielded an output vector with n entries, every other value was taken,

which reduced the row vector placed in the A matrix to a length of N entries. Each row represented the change in velocity distribution from the design condition to the altered condition for the given twist distribution.

$$A = \begin{bmatrix} \Delta v_{\theta_1,1} & \Delta v_{\theta_2,1} & \cdots & \Delta v_{\theta_N,1} \\ \Delta v_{\theta_1,2} & \Delta v_{\theta_2,2} & & \\ \vdots & & \ddots & \vdots \\ \Delta v_{\theta_1,N} & \Delta v_{\theta_2,N} & \cdots & \Delta v_{\theta_N,N} \end{bmatrix} \tag{73}$$

With all the matrices populated, it is possible to solve for x by multiplying both sides of Equation 72 by the inverse of A. For the sake of robustness, the pseudo-inverse was used instead of the true inverse, as the A-matrix tended to be near singular.

$$\vec{x}_{diff} = A^{-1}\vec{b} \tag{74}$$

Recall that this x-vector is of length N, while the rotor contains n radial stations. In order to obtain values for the remaining stations, a linear interpolation was used in between each point to create a new, complete x-vector. Again, $\vec{x}$ corresponds to the value of incidence at each radial station that needs to be added to the original design twist, so the final twist distribution can be defined according to Equation 75.

$$\vec{x}_{desired} = \vec{x}_{baseline} + \vec{x}_{diff} \tag{75}$$

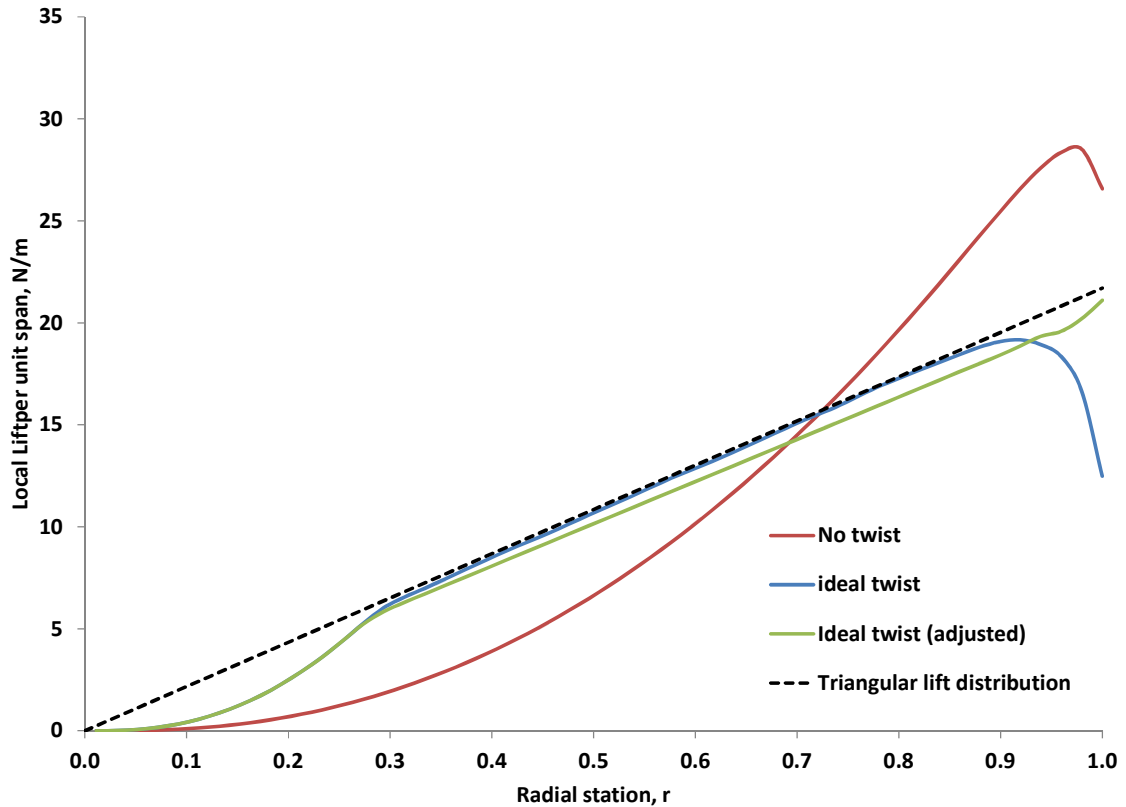We can see an example of how this method can be used in Figure 41.

Figure 41: Matching triangular lift distribution

The dotted line shows the lift triangular distribution that would result from a rotor

operating with a constant inflow velocity. If the rotor is ideally twisted and then analyzed

using QPROP, it will experience lift degradation at the rotor tips due to three-dimensional

effects. However, using the aforementioned method, the twist can be modified to account

for these effects, and bring the predicted lift distribution back much closer to its intended

shape. Analysis has suggested that there is not much to be gained in terms of power

savings, however, the ability to manipulate the rotor while incorporating three-

dimensional effects could prove useful in terms of structural considerations. From this

figure we can see that compared to the untwisted case, the twisted rotors shift a

significant part of the lift away from the tip and towards the root. This decreases the

bending moment seen by the entire rotor, meaning that the rotor structure could either be

made lighter to yield the same deflection, or not changed and deflect less. The downside is that it is computationally expensive, and therefore should likely be used in later phases of the design.

Creating the chord distribution by means of the solidity
The rotor solidity, σ, is defined as the ratio of rotor blade area to rotor disc area, which can be expressed according to Equation 76.

$$\sigma = \frac{N\int_0^R c(r)dr}{\pi R^2} \qquad (16)$$

For a constant-chord rotor, this reduces to Equation 77

$$\sigma = \frac{Nc}{\pi R} \qquad (77)$$

It was shown that an optimally tapered blade $\left(c = \frac{c_t}{r}\right)$ is not realizable at the root, and therefore a maximum chord value must be established. If we label this value c_{max} and define r_{max} as the radial station at which c_{max} is first reached, then Equation 78 must hold.

$$c_t = c_{max}r_{max} \qquad (78)$$

Accordingly, the solidity for a practically optimal rotor is calculated using Equation 79.

$$\sigma = \frac{Nc_t}{\pi R}[1 - \ln(r_{max})] \qquad (79)$$

For the single-taper blade, two variables must be predetermined in order to find a suitable chord distribution. Although there are three relevant variables (c_t, c_r, Λ), they are related by expression $\Lambda = \frac{c_r}{c_t}$, which eliminates the need to initially define all three. As was done

with the optimally tapered blade, it may be necessary to set a maximum allowable chord value. If the desired solidity cannot be obtained with taper that extends the entire length of the rotor, then a constant-chord inboard section will be required, again similar to the optimally tapered rotor. Using the same notation as presented in Equation 78, the solidity for a single-taper rotor can be found with Equation 80.

$$\sigma = \frac{Nc_t\left[\Lambda r_{max} + \left(\frac{1+\Lambda}{2}\right)(1-r_{max})\right]}{\pi R} \tag{80}$$

One can see that if the rotor is tapered over the entire span $(r_{max} = 0)$, Equation 80 reduces to Equation 81.

$$\sigma = \frac{Nc_t\left(\frac{1+\Lambda}{2}\right)}{\pi R} \tag{81}$$

Similarly, if the rotor has a constant chord for the entire span $(r_{max} = 1 \ and \ \Lambda = 1)$, then both Equation 80 and Equation 81 will reduce to Equation 82, which is the same result we obtained with Equation 77.

$$\sigma = \frac{Nc}{\pi R} \tag{82}$$

Conversely, it is possible to create a chord distribution that will yield a desired rotor solidity. The non-tapered blade is most obvious, as Equation 82 simply can be manipulated to take the form seen in Equation 83.

$$c = \frac{N\sigma_{desired}}{\pi R} \tag{83}$$

The chord distribution for an optimal rotor was already discussed, but it is presented here in a more succinct form:

$$c = \begin{cases} c_{max}, & r \leq r_{max} \\ \dfrac{c_t}{r}, & r > r_{max} \end{cases} \tag{84}$$

$$where \; r_{max} = \frac{c_t}{c_{max}}$$

The single-taper blade requires multiple steps to calculate the chord distribution, because in order to maintain the desired taper while still achieving the specified solidity, the chord might tend to exceed the previously defined maximum chord value.

We can find the maximum possible solidity for which the rotor could be tapered for the entire span by using Equation 85.

$$\sigma_{max} = \frac{N(1+\Lambda)c_{max}}{2\Lambda\pi R} \tag{85}$$

If the desired solidity is less than or equal to this value, the tip and root chords could be defined according to Equation 86 and Equation 87, respectively.

$$c_t = \frac{2\pi R \sigma_{desired}}{N(1+\Lambda)} \tag{86}$$

$$c_r = \Lambda c_t \tag{87}$$

However, if the desired solidity exceeds this value, then the rotor will have to remain constant at c_{max} from the root until some place along the span, r_{max} , after which the rotor can taper for the remainder of the span. In order to calculate r_{max} , the tip chords must be defined according to Equation 88.

$$c_t = \frac{c_r}{\Lambda} \tag{88}$$

Setting the root chord equal to c_{max} , we can calculate r_{max} using Equation 89.

$$r_{max} = \frac{\frac{\pi R \sigma_{desired}}{N} - \left(\frac{c_t + c_{max}}{2}\right)}{\left(\frac{c_{max} - c_t}{2}\right)} \tag{89}$$

The value of r_{max} should range from 0 to 1. If it is less than 0, then the rotor should be able to be tapered its entire length, and therefore the value r_{max} is not relevant. Similarly, if it is greater than 1, the desired solidity is greater than the maximum possible solidity, and thus the value r_{max} is again of no consequence. Assuming that this value falls within the acceptable domain, the chord will be fixed at c_{max} from the root until r_{max} , and will then taper to the tip of the rotor.

Rotor inflow velocity, v
In order for the rotor to be operating at point of minimum induced power, a constant inflow velocity ratio—and hence a constant inflow velocity—is desired. This is proved using the calculus of variations. The induced power is proportional to the kinetic energy of the rotor wake. Writing the induced velocity as a mean value $\bar{v}$ plus a perturbation δv the proof can be demonstrated through Equations 90-93:

$$KE \sim \int v^2 dA \tag{90}$$

$$v = \bar{v} + \delta v \tag{91}$$

$$\int \delta v dA = 0 \tag{92}$$

$$\int v^2 dA = \bar{v}^2 A + \int (\delta v)^2 dA \tag{93}$$

Clearly for a minimum kinetic energy, the perturbation value δv must be zero, which implies that the induced velocity is constant over the entire rotor.

Rotor twist for constant inflow velocity

Achieving this desired velocity is possible through the use of rotor twist, although the twist required will always be nonlinear. The simplest case is that of the constant chord rotor, for which the twist distribution follows Equation 94. This is referred to as ideal twist.

$$\theta = \frac{\theta_t}{r} \tag{94}$$

While this twist distribution is not recognizable near the root, it will yield a uniform induced velocity over nearly the entire rotor. Analysis suggests that for the inboard 25% of the rotor, a non-uniform velocity produces negligible power increases. Theoretically, a uniform velocity distribution can be realized for any rotor geometry. Blade element theory gives the rotor thrust coefficient as Equation 95.

$$C_T = \int_0^1 \frac{\sigma}{2} \left[C_{l_\alpha}(\theta r^2 - \lambda r) + C_{l_0} r^2 \right] dr \tag{95}$$

Accordingly, the differential thrust coefficient can be examined at each radial station using Equation 96-99.

$$dC_T = \frac{\sigma}{2} \left[C_{l_\alpha}(\theta r^2 - \lambda r) + C_{l_0} r^2 \right] \tag{96}$$

$$dC_T = \frac{\sigma}{2} \left[C_{l_\alpha} \left(\theta - \frac{\lambda}{r} \right) r^2 + C_{l_0} r^2 \right] \tag{97}$$

$$dC_T = \frac{\sigma}{2} \left[\left(C_{l_\alpha} \alpha + C_{l_0} \right) r^2 \right] \tag{98}$$

$$dC_T = \frac{\sigma}{2} \left[C_l r^2 \right] \tag{99}$$

At the rotor tip, where r=1, the expression reduces to Equation 100.

$$dC_{T_t} = \frac{\sigma_t}{2} C_{l_t} \tag{100}$$

The quantity σ_t does not have any physical significance, as the solidity only applies to the entire rotor. However, it represents the relationship between local chord and total rotor radius, as depicted by Equation 101.

$$\sigma_t = \frac{Nc_t}{\pi R} \qquad (101)$$

A uniform inflow velocity yields a triangular lift distribution. Therefore the differential thrust coefficient can be related to the tip coefficient according to Equation 102.

$$dC_T = dC_{T_t} r \qquad (102)$$

Integrating Equations 99, 100, and 102, we obtain Equation 103.

$$\frac{\sigma}{2}[C_l r^2] = \frac{\sigma_t}{2} C_{l_t} r \qquad (103)$$

Equation 104 delivers the lift coefficient at any point along the rotor, assuming that the rotor geometry is known.

$$C_l = \frac{\sigma_t}{\sigma} \frac{C_{l_t}}{r} \qquad (104)$$

Equating this to the original expression for the lift coefficient, which appears in Equation 105, the twist distribution to yield a constant inflow velocity is determined by Equation 106. When applied to an optimum chord distribution, this twist will yield a constant lift coefficient over the entire rotor; it is then called an optimum twist distribution.

$$C_l = C_{l_\alpha}\left(\theta - \frac{\lambda}{r}\right) + C_{l_0} \qquad (105)$$

$$\theta = \frac{\frac{\sigma_t}{\sigma} \frac{C_{l_t}}{r} - C_{l_0}}{C_{l_\alpha}} + \frac{\lambda}{r} \qquad (106)$$

92

Appendix D: Routh's Discriminant Hand Calculations

Here we are solving for Routh's Discriminant in order to determine where the rotor should be placed to eliminate any unstable oscillation[14]. Earlier, this discriminant was reduced to the following equation for the situation we are considering.

$$R.D. = -\left(\frac{g}{I_{yy}}\frac{\partial M}{\partial \dot{x}}\right)$$

We know that g and I_{yy} will both be positive, therefore we must solve for $\frac{\partial M}{\partial \dot{x}}$, which can be expanded as follows:

$$\frac{\partial M}{\partial \dot{x}} = \frac{dM}{da_{1_s}}\frac{\partial a_{1_s}}{\partial \mu}\frac{\partial \mu}{\partial \dot{x}} - \frac{\partial X}{\partial \dot{x}}h_M$$

Using the definition of each coefficient and inserting values corresponding to *Da Vinci III*'s geometry, we obtaining the proceeding expressions:

$$\frac{\partial M}{\partial a_{1_s}} = \frac{\frac{3}{4}eA_b\rho(\Omega R)^2 a}{\gamma}$$

$$\gamma = \frac{\rho a c R^4}{I_b}$$

$$\frac{\partial a_{1_s}}{\partial \mu} = \frac{8}{3}\theta_0 + 2\theta_1 - 2\frac{v_1}{\Omega R}$$

$$\frac{\partial \mu}{\partial \dot{x}} = \frac{1}{\Omega R}$$

$$\frac{\partial X}{\partial \dot{x}} = -\rho A_b(\Omega R)^2\frac{\partial C_H/\sigma}{\partial a_{1_s}}\frac{\partial a_{1_s}}{\partial \mu}\frac{\partial \mu}{\partial \dot{x}}$$

$$\frac{\partial\ C_H/\sigma}{\partial a_{1_s}} = \frac{3}{2}\left(C_T/\sigma - \frac{a}{18}\theta_{.75}\right)$$

$$\frac{\partial a_{1_s}}{\partial q} = -\frac{16}{\gamma\Omega\left(1 - \frac{e}{R}\right)^2}$$

$$A_b = 414.8\ ft^2$$

$$\sigma = 0.0502$$

$$C_T/\sigma = 0.12212$$

$$\theta_1 = -8° = -0.1396 rad$$

$$\theta_{.75} \cong 6° = 0.1047\ rad$$

$$e = 2ft$$

$$v_1 = 2.4819$$

$$h_M = 2$$

$$a \cong 6$$

$$\Omega = 0.8901\ rad/s$$

$$\Omega R = 44.5059$$

$$\bar{c} = \frac{\sigma\pi R}{N} = 4\ ft$$

$$I_b = \frac{1}{24}m(\bar{c}^2 + (2R)^2) - \frac{1}{25}m(\bar{c}^2 + (2e)^2)$$

$$I_b = 387.63 \; slugs \; ft^2$$

We can now begin to place the newly determined coefficients back into our original equation.

$$\frac{\partial M}{\partial \dot{x}} = \frac{dM}{da_{1_s}} \frac{\partial a_{1_s}}{\partial \mu} \frac{\partial \mu}{\partial \dot{x}} - \left(\frac{\partial X}{\partial \dot{x}}\right) h_M$$

$$\frac{\partial M}{\partial \dot{x}} = \frac{dM}{da_{1_s}} \frac{\partial a_{1_s}}{\partial \mu} \frac{\partial \mu}{\partial \dot{x}} + \rho A_b (\Omega R)^2 \frac{\partial \, C_H/\sigma}{\partial a_{1_s}} \frac{\partial a_{1_s}}{\partial \mu} \frac{\partial \mu}{\partial \dot{x}} h_M$$

$$\frac{\partial M}{\partial \dot{x}} = \frac{\partial a_{1_s}}{\partial \mu} \frac{\partial \mu}{\partial \dot{x}} \left[\frac{dM}{da_{1_s}} + \rho A_b (\Omega R)^2 \frac{\partial \, C_H/\sigma}{\partial a_{1_s}} h_M \right]$$

$$\frac{\partial M}{\partial \dot{x}} = k_1 \left[\frac{\frac{3}{4} e A_b \rho (\Omega R)^2 a}{\gamma} + \rho A_b (\Omega R)^2 \frac{3}{2} \left(C_T/\sigma - \frac{a}{18} \theta_{.75} \right) h_M \right]$$

$$\frac{\partial M}{\partial \dot{x}} = k_1 \frac{3}{4} A_b \rho (\Omega R)^2 \left[\frac{ea}{\gamma} + 2 \left(C_T/\sigma - \frac{a}{18} \theta_{.75} \right) h_M \right]$$

$$\frac{\partial M}{\partial \dot{x}} = k_2 \left[\frac{ea}{\frac{\rho a c R^4}{I_b}} + 2 h_M \left(C_T/\sigma - \frac{a}{18} \theta_{.75} \right) \right]$$

$$\frac{\partial M}{\partial \dot{x}} = k_2 \left[\frac{e I_b}{\rho c R^4} + 2 h_M \left(C_T/\sigma - \frac{a}{18} \theta_{.75} \right) \right]$$

$$\frac{\partial M}{\partial \dot{x}} = k_2 (0.0130 + 0.1744 h_M)$$

$$\boldsymbol{h_M} < -0.90 \; in \; \longrightarrow \; \frac{\boldsymbol{\partial M}}{\boldsymbol{\partial \dot{x}}} < 0$$

We see that a rotor placed in a plane at least -0.90 inches above the helicopter center of gravity should eliminate any unstable rotor oscillations.